Occurrence of partial and total coseismic ruptures of segmented normal fault systems: insights from the Central Apennines, Italy.

Francesco Iezzi[1*], Gerald Roberts[1], Joanna Faure Walker[2], Ioannis Papanikolaou[3]

[1]Department of Earth and Planetary Sciences, Birkbeck, University of London, Malet Street, London, WC1E 7HX, UK

[2] Institute for Risk and Disaster Reduction, University College London, Gower Street, London, WC1E 6BT, UK

[3]Mineralogy-Geology Laboratory, Department of Natural Resources Development and Agricultural Engineering, Agricultural University of Athens, 75 Iera Odos, 118-55 Athens, Greece

*Corresponding author: Francesco Iezzi, francesco.iezzi.15@ucl.ac.uk, +447928037318, Department of Earth and Planetary Sciences, Birkbeck, University of London, Malet Street, London, WC1E 7HX, UK

Abstract

Normal faulting earthquakes rarely rupture the entire extent of active normal faults, and can also jump between neighbouring faults. This confounds attempts to use segmentation models to define the likelihood of future rupture scenarios. We attempt to study this problem comparing the offsets produced in single earthquakes with those produced by multiple earthquakes over longer timescales, together with detailed studies of the structural geology.

We study the active normal fault system causative of the Mw 6.3 2009 L'Aquila earthquake in central Italy, comparing the spatial distribution of coseismic offsets, cumulative offsets that have developed since 15 ±3 ka, and the total offsets that have accumulated since the faults initiated at 2-3 Ma. Our findings suggest that: 1) faults within a segmented fault system behave as a single interacting fault segment over time periods including multiple earthquake cycles (e.g. 2-3 Ma or 15±3ka), with single earthquakes causing either partial or total ruptures of the entire system; 2) an along-strike bend causes throw and throw-rates enhancements within the bend throughout the seismic history of the fault system. We discuss the synchronised and geometrically controlled activity rates on these faults in terms of the propensity for floating earthquakes, multi-fault earthquakes, and seismic hazard.

1. Introduction

Normal faulting earthquakes commonly occur within fault systems that consist of multiple closely-spaced fault surfaces, both along and across strike (Jackson et al., 1982; Crone et al., 1987; dePolo et al., 1991; Suter, 2015; Civico et al., 2018; Villani et al., 2018). The summed slip across all the faults that developed over the entire history of faulting (herein defined as long-term slip, also known as total or finite slip) commonly displays a coherent pattern with a slip maxima decreasing along strike to zero at the overall tips of the system (e.g. Roberts and Michetti, 2004). However, some earthquakes can float along a single fault within the system, rupturing either small portions or the entire length of the fault (Visini et al., 2019), whilst others rupture several faults during a single seismic event producing multi-fault earthquakes (also known as multi-rupture or multi-segment earthquakes) (Caskey and Wesnousky, 1996; Morewood and Roberts, 2001; Suter, 2015; Brozzetti et al., 2019). Hence, it can be unclear how the coseismic slip distribution in one earthquake relates to the summed long-term slip distribution. This uncertainty in the relationship between coseismic slip and longer-term slip is important because it limits our ability to plan for specific coseismic slip distributions and expected earthquake magnitudes during seismic hazard assessment given knowledge of the longer-term faulting. In this paper we attempt to show some key features involved in this process, relating long-term slip magnitudes to fault geometries such as along-strike bends, highlighting the fact that coseismic ruptures do not necessarily inhabit the whole fault length or reflect the location of maximum strain accumulation in the longer term.

For example, during the 2016-2017 Central Italy seismic sequence (Chiaraluce et al. 2017), two large earthquakes with different magnitudes ruptured the network of faults that comprise the Mt. Vettore normal fault system in central Italy (Figure 1). The 24th August 2016 M_w 6.0 earthquake ruptured the ground surface along the SE end of the fault system (Figure 1a.i; Livio et al., 2016). Only 67 days later, following a M_w 6.2 event on the 26th October, the 30th October 2016 M_w 6.5 earthquake re-ruptured the same location as the 24th August event, but also propagated further along strike, rupturing what appears to be almost the entire extent of the Mt. Vettore fault system (Figure 1a.ii; Civico et al., 2018; Villani et al., 2018; Brozzetti et al., 2019). In an attempt to constrain the long-term slip-distribution of the fault system that ruptured in these earthquakes, and how this relates to single ruptures, Iezzi et al. (2018) mapped the ruptures and constructed geological cross-sections that showed that the total along strike length of the fault system is ~27.5 km (Figure 1b.i). The 24th August 2016 M_w 6.0 earthquake produced surface ruptures along a single fault in the system for ~5 km along strike from the SE tip, accounting only for the ~18% of the total fault system length. In contrast, the 30th October 2016 M_w 6.5 earthquake ruptured what appears to be the entire length of the fault, and several faults within the system, revealed by comparison between the geological throw and the surface traces of the coseismic ruptures (Figure 1b). It is noteworthy that the maximum coseismic slip for both the earthquakes was located within an along-strike fault bend, where the longer term cumulative geological throw increases to the maximum value of ~1400m producing marked asymmetry in that throw profile (Figure 1b).

The key observations from the 2016 Mt. Vettore examples are that (1) the longer-term slip is asymmetric, with the largest offset (~1400 m) within an along-strike fault bend (Figure 1b.i; Iezzi et al., 2018); (2) the coseismic throw profiles for both earthquakes were also asymmetric, but with opposite senses (either skewed to the NW or SE), with the largest offsets (~30 cm and ~234 cm) located within the same along-strike fault bend (Figures 1b.ii and 1b.iii; Iezzi et al., 2018); (3) multiple fault strands were activated in single earthquake (e.g. the 30th October 2016 Mw 6.5 earthquake; Ferrario and Livio, 2018), contributing to the long-term throw. Thus, the along-strike fault bend, and associated multiple fault strands, appear to be a recurrent control on slip that produces the long-term slip distribution. Although bends are commonly considered locations where the propagation of ruptures stop (Biasi and Wesnousky, 2017), the Mt. Vettore example shows that in some cases, propagation of coseismic ruptures across fault bends produces enhancement of slip along the fault bend (Iezzi et al., 2018). Enhancement of slip within along strike fault bends on single normal faults has been reported from previous coseismic slip distributions for single earthquakes (e.g. Mildon et al. 2016) and from time periods containing multiple earthquakes such as the time period since the last glacial maximum (LGM, 15 ± 3ka; Wilkinson et al. 2015). Faure Walker et al. (2009) provide quantitative descriptions of why slip enhancement is expected within along strike fault bends along single normal faults, showing that across an along-strike fault bend the throw rate must vary in order to conserve the strain rate along the fault and within the fault bend, due to spatial changes in the strike and dip of the fault, but constant horizontal extension. Less is known about slip enhancement across along strike bends where multiple faults are involved.

In this paper we ask whether activation of multiple faults during single earthquakes and the largest long-term and coseismic offsets within fault bends, as described for the Mt. Vettore earthquakes, can be identified for other normal faulting examples where multiple faults were involved. We study the 6th April 2009 Mw 6.3 L'Aquila earthquake that occurred 50 km to the SW of the 2016 earthquakes on the Mt. Vettore fault. We show that (1) the long-term slip is again asymmetric, (2) the strike of the multiple fault strands in the area change across a zone defining an along-strike bend in the fault system, (3) the long-term slip maximum is located within the fault bend, (4) in contrast to the 2016 earthquakes, the 2009 ruptures occurred outside the bend so that the location of maximum coseismic slip does not match the location of longer-term maximum fault slip, and (5) a previous earthquake on this fault system in 1703 AD appears to have had an alternative geometry and spatial extent. We discuss the complexity exhibited by the 3 modern earthquake ruptures in April 2009, August 2016 and October 2016, and that in 1703 AD, to investigate if rupture extent in one earthquake can be a good guide to the ruptures that may occur in the longer-term history of an individual fault. Moreover, we discuss how this complexity, in particular with regard to along-strike fault bends, should be taken in account for seismic hazard assessments and when attempting to study the growth of normal faults.

2. Geological background

The 2009 L'Aquila earthquake ruptures occurred in the Aterno Valley, a narrow NW-SE trending tectonic depression located in the central part of the Apennines chain, central Italy

(Figure 2). The Apennines are a formerly-active fold-and-thrust belt, with NE-directed shortening, mainly in Miocene in times, that in general overthrust Mesozoic and Cenozoic limestones onto Miocene flysch deposits (Anderson and Jackson, 1987; Doglioni, 1993). By the late-middle Pliocene (last 2-3 Ma), SW-NE directed extension began in the Apennines (Cavinato and De Celles, 1999; Roberts et al., 2002), causing the growth of a NW-SE normal fault system in this new stress field (Patacca et al., 1990; Pizzi and Scisciani, 2000; Cavinato et al., 2002; Pizzi and Galadini, 2009). The active normal faults are organized with both en-echelon and end-on along-strike arrangements, have lengths of ~20-40 km, and show overall pure dip-slip faulting, with a mean fault slip direction of 222º±4º (Roberts and Michetti, 2004).

Studies of fault scarps on the active normal faults that survived since erosion rates decreased during the demise of the LGM (15 ±3ka) suggest that these faults have throw-rates up to 1.5 mm/yr (Roberts and Michetti, 2004; Papanikolaou et al., 2005; Faure Walker et al., 2010, 2012). Fault-specific earthquake recurrence times are of the order of hundreds to thousands of years (Pace et al., 2006; Galli et al., 2008), and the faults are considered to have the potential to release earthquakes of magnitude up to M_w 7.0 (Blumetti et al., 1993; Cello et al., 1997; Galadini & Galli, 2000; Boncio et al., 2004). Calculations of the extension rate across the central Apennines using fault slip data show regional horizontal extension occurring at up to ~3mm/yr, matching estimates made with geodesy and seismic moment summations (Faure Walker et al., 2010, 2012; D'Agostino et al. 2011). Calculations of the extension rate since 15±3 ka also prompt the idea that earthquake slip is related to dynamic topographic effects that induce slip on viscous shear zones that form the roots of the upper crustal brittle faults (Cowie et al., 2013). This study showed that rates of slip measured across brittle faults at the surface, when averaged over 15 ±3 ka and across the strike of parallel faults, imply along-strike variations in horizontal strain-rates that correlate with along-strike elevation changes. The correlation shows a power-law relationship, mimicking power law viscous flow laws for crustal materials, where strain-rate is proportional to the topographic elevation (stress driver) raised to a power, n = 3. In turn this implies that (1) dynamic topographic effects drive the extension by activating slip in underlying viscous shear zones that drive the rates of overlying earthquake slip, and (b) 15 ± 3 ka is a time period that appears long enough to reveal the longer-term behaviour of the fault system.

With this rheological framework in mind, we note that on the 6th April 2009, the Aterno Valley was struck by a M_w 6.3 earthquake, which caused severe damage to the city of L'Aquila and surrounding villages, with 309 fatalities, followed on the 7th April 2009 by a M_w 5.6 aftershock (Figure 2; Chiaraluce et al., 2011). Seismological and geodetic data suggest a slip distribution with a SE-striking, SW-dipping, 12-19 km long rupture extent at depth (Atzori et al., 2009; Walters et al., 2009; Cheloni et al., 2010; Cirella et al., 2010; Papanikolaou et al., 2010; D'Agostino et al., 2012; Lavecchia et al., 2012). Coseismic surface ruptures showed that the Paganica fault was the fault that ruptured in the earthquake, with maximum measured coseismic offset of about 10 cm (Figures 2 and 3; Falcucci et al., 2009; Boncio et al., 2010; Emergeo Working Group, 2010; Galli et al., 2010; Wilkinson et al., 2010; Vittori et al., 2011). DInSAR analysis exhibited a distributed coseismic slip of 25 cm, possibly including the contribution of the 7th April event to the deformation field (Papanikolaou et al., 2010). DiNSAR analysis also demonstrated that 66% of the deformed area subsided whereas the 34% was uplifted, with an overall footwall uplift versus hangingwall subsidence ratio of about 1/3 (Papanikolaou et al., 2010).

The Paganica fault is characterized by several smaller fault segments that juxtapose Cenozoic limestones and calcarenites with Pleistocene-Holocene deposits (Vezzani and Ghisetti, 1998; ISPRA, 2009; Pucci et al., 2015). Different studies agree that the slip-rate in the Holocene is ~ 0.4 mm/yr (Galli et al., 2010; Roberts et al., 2010; Cinti et al., 2011; Moro et al., 2013). However, we point out that the Paganica fault is only one of a number of faults that deform the region, controlling the geomorphology and contributing to the summed long-term fault slip. In fact, following compilation of palaeoseismic results from trench studies conducted on a number of the faults, Galli et al. (2011) suggested that previous earthquakes, such as the 1703 A.D. Mw 6.7 event, may have ruptured multiple faults within the system (Figure 4). The question arises as to which rupture scenario (compare Figure 4 a and b) should be used to plan for future coseismic slip distributions and expected earthquake magnitudes during seismic hazard assessment. Measurements of the long-term slip, accumulated over the entire activity of the faults, can provide information on whether the faults are interacting over a time span which encompasses all the seismic cycles that the faults have experienced, and therefore it may provide insights into the occurrence of multi-fault earthquakes in the Aterno Valley Fault System. In order to assess whether information on the long-term slip can help with this question we have (1) constructed 39 geological cross-sections across the Aterno Valley Fault System to quantify the along-strike long-term throw profile for the entire fault system (Figures 5a and 5b); (2) made new measurements of post-LGM throw and throw-rates, collated these with published values, and constructed an along-strike profile of the values (Figures 6 and 7); (3) studied the large-scale relief associated with the footwall escarpment of the Aterno Valley Fault System, obtained with topographic profiles derived from 10 m resolution DEM; (4) studied the along-strike arrangements of faults, in order to observe how the fault strike varies along the fault system (Figure 8); (5) compared the longer term throw profile with the distribution of the coseismic ruptures following the 2009

L'Aquila earthquake, in order to better understand the relationships between faults of the Aterno Valley Fault System and the role of the 2009 earthquake in the long-term seismic history of the region (Figure 9).

3. Methods

We have identified fault segments showing evidence of post-LGM and Holocene activity (Figure 2) by combining results from our fieldwork, published geological maps, palaeoseismology, structural geology and high-resolution imagery such as Google Earth^{TM} and a 10 m resolution DEM (opendata.regione.abruzzo.it).

We have constructed 39 approximately serial geological cross-sections across pre-rift strata along the strike of the Aterno Valley Fault System, based on published geological maps and our own mapping (Figures 5a and 5b; Vezzani and Ghisetti, 1998; ISPRA, 2009; Pucci et al., 2015). We use these cross-sections in order to define the long-term slip of the analysed faults, stretching back to 2-3 Ma (Cavinato and De Celles, 1999; Roberts et al., 2002). The cross-sections were constructed perpendicular to the fault traces, in order to avoid measurements of apparent fault dip. The cross-sections were chosen in order to avoid effects of inherited throw associated with cross faults with pre-Quaternary tectonic history (e.g. Pizzi and Galadini, 2009). The long-term throw has been measured as the vertical distance between the hangingwall and footwall cut-offs of the Meso-Cenozoic bedrock formations that were in place before the onset of the extension across the Apennines, and therefore record all the slip accumulated by the faults (since 2-3 Ma). The bedrock formations exhibit significant variability in thickness across the fault system (Vezzani and Ghisetti, 1998). Therefore, to incorporate uncertainty in the thickness of a formation, for example under the sedimentary fill of the Aterno Valley, we considered the maximum stratigraphic thickness provided by Vezzani and Ghisetti (1998), but used local geological observations to gain appropriate values. In places where the fault trace is complex, formed by both synthetic and antithetic fault segments, we considered the total throw as the sum of the single measurements of throw on each fault segment. Some faults present in the geological map have not been included in the Aterno Valley Fault System because a lack of evidence of Holocene or post-LGM activity. Also, some faults with Holocene or post-LGM activity, as revealed by geomorphology and palaeoseismology, may not have been resolved by the geological maps in cases where the thickness of the Meso-Cenozoic units is larger than the fault offset, and therefore there is no evidence of offset of geological units on the fault. We took this into account during our analysis.

We have also collated measurements of the throw accumulated since the demise of the Last Glacial Maximum (15 ±3 ka; LGM throw) from published values and our own field measurements (Figures 6, 7 and Table 1). The LGM was a time of high erosion and sedimentation due to the cold climate and freeze-thaw activity (Tucker et al. 2011). This means that slip in the LGM has not been preserved, and only slip after the climate changed during the demise of the LGM has been preserved as fault scarps. In particular we used the throw values for periglacial slopes from the LGM offset across the faults (see Roberts and Michetti 2004 for a review). Thus, to gain values for the throw-rates on the active fault scarps we have combined (1) measurements of fault scarp offsets (Roberts and Michetti, 2004; Papanikolaou et al., 2005; Faure Walker et al., 2010; Galli et al., 2011), (2) palaeoseismological analysis (Galli et al., 2010; Galli et al., 2011; Cinti et al., 2011), assuming that the throw-rate measured in the trench is constant during the last 15±3 ka, and (3) our own new field measurements (Figure 7) to get slip-rates that apply over all or parts of the Holocene. We have assumed constant fault slip-rates since 15 ±3 ka because *in situ* ^{36}Cl cosmogenic exposure dating shows that this is a good approximation of the time when scarps began to be preserved (Cowie et al., 2017). Our post-LGM throw values have only been collected from locations free of significant Holocene erosion and sedimentation, following the approach of Cowie et al. (2017), where the periglacial surfaces in the footwall and hangingwall are planar and undisturbed by post-Holocene erosion, evidenced by parallel hangingwall and footwall cut-offs (Figure 7c). With these characteristics, we can reasonably assume that the fault scarp has been exhumed only by repeated coseismic surface ruptures, and therefore its height represents a measurement of the throw accumulated since 15±3 ka.

We have also studied the along-strike arrangements of faults, and we have constructed strike lines for the principal fault segments in order to understand how the fault strike varies along the fault system (Figure 8). Strike lines are horizontal lines joining points of the same elevation on a structure such as the hangingwall cut-off.

To compare all the above data, we have constructed along-strike profiles for the long-term throw from offsets of pre-rift strata (Figure 9a), and offsets since the LGM (Figure 9b). These profiles, together with the analysis of the fault traces arrangement, the topographic relief associated with the Aterno Valley Fault System (Figure 9c) and the presence of N-S striking cross faults (e.g. Pizzi and Galadini, 2009; Figure 5), allow us to identify the tips of the fault system and to reconstruct the segmentation of the main faults of the system (Figure 9f). We have also compared the long-term activity of the Aterno Valley Fault System with the coseismic activity following the 6th April M_w 6.3 L'Aquila earthquake and 7th April Mw 5.6 aftershock, herein referred to as (1) the coseismic surface deformation derived from DiNSAR analysis (Figure 9d; Papanikolaou et al., 2010), and (2) five different published geodetic and seismological models of the coseismic slip distribution at depth of the earthquake (Figure 9e; Atzori et al., 2009; Walters et al., 2009; Cheloni et al., 2010; Cirella et al., 2010; D'Agostino et al., 2012).

4. Results

4.1 Analysis of the geometry of the Aterno valley fault system

The Aterno valley fault system is composed of several fault segments of variable length, with both en-echelon and end-on arrangements (Figure 8). Overall, the south-eastern part of the fault system is highly segmented, characterized by relatively short fault traces. The north-western part is characterized by relatively more continuous fault traces, with significant overlaps between fault segments. The distance between the tips of neighbouring faults is relatively small, and in most instances is less than 5 km.

Strike-lines drawn along the fault system show that the fault system contains a bend in its strike (Figure 8). While the fault segments outside the bend (outer faults) have an average strike of N131º, with values ranging between N130º and N133º, across the bend the strike gradually change, with values ranging between N083º and N122º, with an average strike of N106º. This along-strike bend, resulting from a variation of fault strike of ~25º, produces an overall left en-echelon arrangement of the fault system (Figure 8).

4.2 Analysis of the throw profiles of the Aterno valley fault system

By combining the measured along-strike throw distributions and the fault trace arrangements, we have reconstructed the segmentation and the length of the four main faults of the Aterno valley fault system: the Barisciano fault, the Paganica-San Demetrio fault, the Pettino fault and the Barete fault (Figure 9). The Barisciano and the Paganica-San Demetrio faults at the surface appear to be characterised by many relatively short, discontinuous fault segments (Figure 9d), organised with en-echelon arrangements and the presence of mostly synthetic faults with a few short antithetic strands. However, the lengths of individual faults are in places hard to determine due to limited exposure; it may be that faults are more connected than we have shown in Figure 9e. The multi-humped throw profiles, with numerous maxima and minima along strike, are consistent with the notion that the faults grew by linkage of relatively short segments (green and pale blue lines in Figure 9a; see Cowie and Roberts, 2001). The Pettino and Barete faults are characterized by what appear to be longer and more continuous fault segments, although again this may be due to more continuous exposure rather than any difference in fault connectivity compared to faults to the SE (Figure 9e). However, greater connectivity may be reflected in their long-term throw profiles, which show a single maximum and a decrease of values towards the fault terminations (purple and orange lines in Figure 9a).

The cumulative long-term throw profile across all the faults in the Aterno Valley Fault System (dark blue line in Figure 9a) shows that the overall throw is asymmetric, with maximum throw located in the NW half of the overall fault trace, within the along-strike bend of the Aterno Valley Fault System defined by strike lines (Figure 8).

The throw that has accumulated since the demise of the LGM (dark blue line in Figure 9b), constructed using measurements from fault scarp heights (squares in Figure 9b) and palaeoseismology (triangles in Figure 9b), shows that the cumulative post-LGM throw is again asymmetric, with the post-LGM maximum throw located in the NW half of the overall fault trace, within the along-strike bend of the Aterno Valley Fault System defined by strike lines (Figure 8).

The topographic relief associated with the Aterno Valley Fault System agrees with the findings obtained with the study of the longer-term offsets (Figure 9c). The relief achieves a maximum within the bend (~1000 m) and decreases towards zero at the tips of the fault system (Figure 9c). A local minimum within the fault bend is produced by a prominent incised drainage system that cuts through the fault system (see Figure 2).

Overall, the similarity between the long-term and post-LGM throw profiles (Figures 9a and 9b), together with the study of the topographic relief (Figure 9c), indicates that this group of faults behave as a single interacting fault segment over multiple earthquake cycles, and that the repetition of slip during several earthquake cycles, like that occurred since the demise of the LGM, built the long-term throw. This is also suggested by the observation of the slip vector azimuths measured along the fault system (from Roberts and Michetti, 2004; Papanikolaou et al., 2005; Faure Walker et al., 2010), which show a convergent pattern towards the hangingwall, with dip-slip kinematic in the central part and oblique slip towards the tips of the fault system (Figure 9f). Converging slip-vector azimuths like this have been used as a criterion to define the length of single interacting segments because they form due to the lateral continuity of differential uplift between the hangingwall and footwall, which causes asymmetry between the extensional strains in both hangingwall and footwall (Ma and Kusznir, 1995; Roberts 1996a, Roberts and Ganas 2000, Roberts and Michetti 2004, Roberts 2007; Ampel et al., 2013).

4.3 Comparison between the longer-term activity of the Aterno Valley Fault System and the M_w 6.3 L'Aquila Earthquake

The key question is whether the single interacting segment defined above ruptures in its entirety or partially in single earthquakes. When we compare the long-term and the post-LGM throw profiles with the coseismic slip profiles of the 6th April 2009 M_w 6.3 L'Aquila earthquake, it is clear that the earthquake only ruptured a relatively small portion of the Aterno Valley Fault System (~20 km; compares Figures 9a-c and 9d-f), comprising only ~ 40% of its overall ~50 km along strike length. This is consistent with the mapped traces of the coseismic ruptures, which are localized in a small part of the fault system (Figure 9e-f). Note that the surface rupture formed mostly outside of the overall fault bend in the Aterno Valley Fault System, where the maximum cumulative post LGM throw and longer-term throw was observed (Figure 9f).

4.4 Comparison between the long-term and post-LGM throw rates along the Aterno Valley Fault System

To understand how the post-LGM throw rates compare with the long-term history of the fault system, we have calculated the predicted long-term throw profile of the Aterno Valley Fault System assuming constant post-LGM throw rates during the entire fault activity (last 3 Ma; Roberts et al., 2002), and compared it with the long-term throw profile derived from the geological cross-sections (Figure 10). The comparison shows that the predicted long-term throw is overall consistent with the measured long-term throw profile given the above assumptions, and reveals how the post-LGM fault throw rates are working in a way that mimics the long-term behaviour of the fault system. In fact, local discrepancies between the predicted and the measured throw profiles suggest that faults are working in order to produce a throw profile consistent with one for a single interacting fault segment, with relatively low post-LGM throw-rates localized where the long-term throw profile presents local maxima (for example at ~40 km distance along strike, Figure 10) and relatively fast post-LGM throw rates localized where the long-term throw profile presents minima (at ~33km distance along strike, Figure 10).

Thus, our overall finding from this and the previous section is that faults studied herein behave as a single interacting fault segment over time periods containing multiple earthquake cycles (e.g. over 15 ±3ka or 2-3 Ma), with the position of the maximum offset controlled by a bend in the strike of the system, producing an asymmetric throw profile. Individual ruptures float within the fault system, at times rupturing only part of the along strike extent of the system, with other ruptures, such as those in 1703 AD, having a greater along strike extent. Rupture locations since the demise of the LGM may exhibit a propensity to fill displacement deficits that have developed over 2-3 Ma. Palaeoseismic results from Galli et al. (2011) suggest that in some earthquakes multiple faults may be ruptured with rupture extent approaching that of the length of the entire fault system.

5. Discussion

Our observations show that the 2009 L'Aquila M_w 6.3 earthquake shared several of the attributes that we observed for the 2016 Mt. Vettore M_w 6.0 and M_w 6.5 earthquakes: the overall long-term throw profile is asymmetric, as is the post-LGM throw profile, and numerous across-strike fault strands combine to produce these asymmetries. However, the coseismic throws in 2009 L'Aquila earthquake occurred mostly outside of the overall fault bend, in contrast to the Mt. Vettore earthquakes. Overall, these three earthquakes show that the locations of coseismic offsets can define either complete or partial rupture of the overall fault system. The "partial" earthquakes float within the structure in the way described for other earthquakes on normal faults (e.g. Roberts, 1996b; Roberts and Koukovelas, 1996; DuRoss et al., 2016). Given these observations, we recommend that the along strike extents of single coseismic ruptures are not a good guide to describe the lengths of fault segments that develop over multiple seismic cycles, or the potential rupture lengths and earthquake magnitudes for future events.

The relative short distance between fault segments of the Aterno Valley Fault System (mostly <5 km across strike) is interesting to compare with maximum distance for the definition of multi-faulting earthquakes on other fault systems such as the San Andreas fault system in California (e.g. UCERF 3 model, Field et al., 2014; 2015; 2017). Empirical studies have also shown that normal faulting earthquakes are capable of rupturing steps in the fault strike that can reach up to 5-7 km (Wesnousky, 2008), and that in dip slip ruptures the 30% of the observed ruptured steps are larger than 5 km (Biasi and Wesnousky, 2016). Moreover, there are examples of normal faulting earthquakes that ruptured simultaneously parallel faults spaced about 5 km (e.g. the M 7.2-6.8 1954 Fairview Peak-Dixie Valley and the M 7.5 1959 Hebgen Lake earthquakes; dePolo et al., 1991). Therefore, the relatively small across strike spacing within the Aterno Valley Fault System may indicate that ruptures can cross between fault strands. Given these considerations, we suggest that for the Aterno Valley Fault System, seismic ruptures appear to be able to jump from one fault to another, rupturing more than one fault during the same seismic event and producing multi-fault earthquakes, as it is suggested from palaeoseismological studies (Galli et al., 2011; see Figure 4a), although data for the

Barisciano fault is lacking. Ruptures within the bend may lead to relatively large throws, for example related to larger coseismic throw, as was the case for the 2016 Mt. Vettore ruptures (Iezzi et al., 2018; Figure 1). If ruptures join along strike linking separate faults, earthquake magnitudes larger than the M_w 6.3 of the 2009 L'Aquila earthquake may occur (e.g. the 1703 earthquake). The worst-case scenario, in which the fault system ruptures for its entire length of about 50 km, would imply that the fault system has the potential to release a M_w 7 earthquake, according to empirical M_w/surface rupture length scaling relationship (Figure 11; Wells and Coppersmith, 1994). More work is needed to assess whether the above is true of other parts of the overall Central Apennines Fault System, but we note that the faults are commonly interconnected and close to each other (Roberts and Michetti 2004). We suggest that the occurrence of multi-fault earthquakes should be investigated for other localities along the fault system, and that study of the structural geology of active faults, as demonstrated in this paper, should form part of future studies aimed at ascertaining the propensity for multi-fault earthquakes.

Our results for the 2016 Mt. Vettore earthquakes and the 2009 L'Aquila earthquake also have implications for how to interpret palaeoseismic results. We show that maximum throw values are found within the bends in both fault systems: for the 2009 L'Aquila earthquake in both the long-term throw and the post-LGM throw profiles, and for the 2016 Mt. Vettore earthquakes in both the long-term and coseismic throw profiles. This is similar to results from other studies which show that anomalously large throws are located within along-strike fault bends on single fault segments (Faure Walker et al., 2009; Wilkinson et al., 2015; Mildon et al., 2016; Iezzi et al., 2018). If high values for throw-rates in the long-term are produced by large values of coseismic throw, rather than more frequent earthquakes, as suggested by the Mt. Vettore example, then palaeoseismic throws reported from trench sites within bends may overestimate the palaeoearthquake magnitude if that value of coseismic throw is used within the scaling relationships between maximum displacement and magnitude, such as that in Wells and Coppersmith (1994), and Manighetti et al. (2007) (Iezzi et al. 2018). In fact, this may well be a common feature for normal fault systems because we note that consistency of the locations of the maxima in both the long-term and LGM throw profiles may indicate that the effect of the along-strike fault bend persists through time (see Faure Walker et al., 2009).

Overall, our results suggest that the 2009 M_w 6.3 L'Aquila earthquake represents a partial rupture of a more complex fault system. Therefore, we recommend that future studies of the Aterno Valley Fault System should investigate whether it has the potential to release larger earthquakes. If this typifies other active normal faults, the occurrence of partial and complete rupture of the overall fault length will produce ambiguity in the outputs of palaeoseismology for seismic hazard. Detailed palaeoseismological studies within segmented fault systems, concentrating on whether multiple faults rupture simultaneously, should be given high priority.

6. Conclusions

We have studied the fault geometry and the slip history of the Aterno Valley Fault System (Central Apennines), ruptured during the 6th April 2009 M_w 6.3 L'Aquila earthquake, in order to understand 1) how coseismic slip magnitudes in one earthquake relate to the summed slip across all the faults of the fault system that have developed over the entire history of faulting and 2) if prominent along-strike bends within a fault system has consistently halted earthquake ruptures or promoted high values of slip.

The comparison between the offset measured since initiation of faulting at 2-3 Ma, since the Last Glacial Maximum at ~15±3 ka and during the 2009 M_w 6.3 L'Aquila earthquake, together with the analysis of the geometry of the fault system and the comparison between long-term and post-LGM throw rates, suggest that: 1) faults within a segmented fault system can behave as a single interacting fault segment over time periods containing multiple earthquake cycles (e.g. over 15 ±3ka or 2-3 Ma), with maxima values of throw within a bend in the strike of the fault system, across which the strike shifts of ~25º; 2) single earthquakes can float within the fault system, rupturing either part or all the along strike extent of the system; 3) the along-strike bend seems to exert a persistent control on the distribution of throw within the fault system, promoting high values of throw and throw-rates within the bend; 4) the close proximity between mapped fault segments indicates that for the Aterno Valley Fault System seismic ruptures may be able to jump from one fault to another, producing multi-fault earthquakes, which can release earthquakes with magnitudes up to M_w 7.

Given the structure of the Central Apennines Fault System, where faults are commonly interconnected and close to each other, we suggest that the occurrence of multi-fault earthquakes should be investigated for other parts of the fault system. Hence, we suggest that study of the structural geology of active faults should be included in assessments of the propensity for the occurrence of multi-fault earthquakes.

Acknowledgments

We thank the Editor Stephen Laubach and three anonymous reviewers for the helpful comments that sensibly improved our paper. This study was funded by NERC Standard Grant

NE/I024127/1 and NERC Studentship to Iezzi. The research data used in this work are all exhibited in the paper.

References

Anderson, H, and J. Jackson (1987), Active tectonics of the Adriatic Region. Geophys J Int; 91 (3): 937-983. doi: 10.1111/j.1365-246X.1987.tb01675.

Atzori, S., I. Hunstad, M. Chini, S. Salvi, C. Tolomei, C. Bignami, S. Stramondo, E. Trasatti, A. Antonioli, and E. Boschi (2009), Finite fault inversion of DInSAR coseismic displacement of the 2009 L'Aquila earthquake (central Italy), Geophysical Research Letters, vol. 36, L15305, doi:10.1029/2009GL039293.

Biasi, G.P and Wesnousky, S.G. (2016), Steps and Gaps in Ground Ruptures: Empirical Bounds on Rupture Propagation, Bulletin of the Seismological Society of America 106, 1110-1124.

Blumetti, A. M., F. Dramis, and A.M. Michetti (1993), Fault-generated mountain fronts in the central apennines (Central Italy): Geomorphological features and seismotectonic implications. Earth Surf. Process. Landforms, 18: 203–223. doi:10.1002/esp.3290180304.

Blumetti, A. M., P. Di Manna, V. Comerci, L. Guerrieri, and E. Vittori (2017), Paleoseismicity of the san demetrio ne'Vestini fault (L'Aquila basin, Central Italy): implications for seismic hazard, Quaternary International, 451, 129-142.

Boncio, P., A. Pizzi, F. Brozzetti, G. Pomposo, G. Lavecchia, D. Di Naccio, and F. Ferrarini (2010), Coseismic ground deformation of the 6 April 2009 L'Aquila earthquake (central Italy, Mw 6.3), Geophysical Research Letters, vol. 37, L06308, doi:10.1029/2010GL042807.

Boncio, P., G. Lavecchia, and B. Pace (2004), Defining a model of 3D seismogenic sources for Seismic Hazard Assessment applications: The case of central Apennines (Italy), J. Seismol., 8(3), 407–425, doi:10.1023/B:JOSE.0000038449.78801.05.

Brozzetti, F., P. Boncio, D. Cirillo, F. Ferrarini, R. de Nardis, A. Testa, F. Liberi and G. Lavecchia (2019), High□resolution field mapping and analysis of the August– October 2016 coseismic surface faulting (central Italy earthquakes): Slip distribution, parameterization, and comparison with global earthquakes, Tectonics, 38, 417–439. https://doi.org/10.1029/ 2018TC005305

S. J. Caskey and S. G. Wesnousky (1997), Static stress changes and earthquake triggering during the 1954 Fairview Peak and Dixie Valley earthquakes, central Nevada, Bulletin of the Seismological Society of America ; 87 (3): 521–527.

Cavinato, G. P., and PG De Celles (1999), Extensional basins in the tectonically bimodal central Apennines fold-thrust belt, Italy: response to corner flow above a subducting slab in retrograde motion, Geology 27, no. 10; 955-958.

Cavinato, G. P., C. Carusi, M. Dall'Asta, E. Miccadei and T. Piacentini (2002), Sedimentary and tectonic evolution of Plio–Pleistocene alluvial and lacustrine deposits of Fucino Basin (central Italy). Sedimentary Geology, 148(1), 29-59, http://dx.doi.org/10.1016/S0037-0738(01)00209-3.

Cello, G., S. Mazzoli, E. Tondi, and E. Turco (1997), Active tectonics in the central Apennines and possible implications for seismic hazard analysis in peninsular Italy, Tectonophysics, *272*(1), 43-68. http://dx.doi.org/10.1016/S0040-1951(96)00275-2

Cheloni, D., N. D'agostino, E. D'anastasio, A. Avallone, S. Mantenuto, R. Giuliani, M. Mattone, S. Calcaterra, P. Gambino, D. Dominici, and F. Radicioni (2010), Coseismic and initial post-seismic slip of the 2009 M w 6.3 L'Aquila earthquake, Italy, from GPS measurements. Geophysical Journal International, 181(3), pp.1539-1546. https://doi.org/10.1111/j.1365-246X.2010.04584.x

Chiaraluce, L., L. Valoroso, D. Piccinini, R. Di Stefano, and P. De Gori (2011), The anatomy of the 2009 L'Aquila normal fault system (central Italy) imaged by high resolution foreshock and aftershock locations, J. Geophys. Res., 116, B12311, doi:10.1029/2011JB008352.

Chiaraluce, L., Di Stefano, R., Tinti, E., Scognamiglio, L., Michele, M., Casarotti, E., et al. (2017), The 2016 Central Italy seismic sequence: A first look at the mainshocks, aftershocks, and source models. Seismological Research Letters, 88(3), 757–771. https://doi.org/10.1785/
0220160221

Cinti, F. R., D. Pantosti, P. M. De Martini, S. Pucci, R. Civico, S. Pierdominici, L. Cucci, C. A. Brunori, S. Pinzi, and A. Patera (2011), Evidence for surface faulting events along the Paganica fault prior to the 6 April 2009 L'Aquila earthquake (central Italy). Journal of Geophysical Research: Solid Earth, 116(B7). 10.1029/2010JB007988

Cirella, A., A. Piatanesi, M. Cocco, E. Tinti, L. Scognamiglio, A. Michelini, A. Lomax, and E. Boschi (2009), Rupture history of the 2009 L'Aquila (Italy) earthquake from non‐linear joint inversion of strong motion and GPS data. Geophysical Research Letters, 36(19). 10.1029/2009GL039795

Civico, R., S. Pucci, F. Villani, L. Pizzimenti, P.M. De Martini, R. Nappi and Open EMERGEO Working Group (2018), Surface ruptures following the 30 October 2016 M w 6.5 Norcia earthquake, central Italy. Journal of Maps, 14(2), pp.151-160.

Cowie, P.A. and G.P. Roberts (2001), Constraining slip rates and spacings for active normal faults. Journal of Structural Geology, 23(12), pp.1901-1915 https://doi.org/10.1016/S0191-8141(01)00036-0

Cowie P. A., R. J. Phillips, G. P. Roberts, K. McCaffrey, L. J. J. Zijerveld, L. C. Gregory, J. Faure Walker, L. N. J. Wedmore, T. J. Dunai, S. A. Binnie, S.P. H. T. Freeman, K. Wilcken, R. P. Shanks, R. S. Huismans, I. Papanikolaou, A. M. Michetti and M. Wilkinson (2017), Orogen-scale uplift in the central Italian Apennines drives episodic behaviour ehavior of earthquake faults, Nature Sci. Rep. 7., 44858; doi:10.1038/srep44858.

D'Agostino, N., Mantenuto, S., D'Anastasio, E., Giuliani, R., Mattone, M., Calcaterra, M., Gambino, P., and Bonci, L. Evidence for localized active extension in the central Apennines (Italy) from global positioning system observations. *Geology*, **39**, 291–294, (2011).

D'Agostino, N., D. Cheloni, G. Fornaro, R. Giuliani, and D. Reale (2012), Space□time distribution of afterslip following the 2009 L'Aquila earthquake, Journal of Geophysical Research: Solid Earth 117, no. B2. 10.1029/2011JB008523

DePolo, C.M., D. G. Clark, D.B. Slemmons, and A. R. Ramelli (1991), Historical surface faulting in the Basin and Range province, western North America: implications for fault segmentation. Journal of structural Geology, 13(2), pp.123-136.

Doglioni, C. (1993), Some remarks on the origin of foredeeps, Tectonophysics, 228(1-2), 1-20.

DuRoss, C. B., S. F. Personius, A. J. Crone, S. S. Olig, M. D. Hylland, W. R. Lund, and D. P. Schwartz (2016), Fault segmentation: New concepts from the Wasatch fault zone, Utah, USA. Journal of Geophysical Research: Solid Earth, 121(2), 1131-1157.

Emergeo Working Group. (2010), Evidence for surface rupture associated with the Mw 6.3 L'Aquila earthquake sequence of April 2009 (central Italy), Terra Nova, 22(1), 43–51. doi:10.1111/j.1365-3121.2009.00915.x

Falcucci, E., Gori, S., Peronace, E., Fubelli, G., Moro, M., Saroli, M., . . . Galadini, F. (2009), The Paganica Fault and surface coseismic ruptures caused by the 6 April 2009 earthquake (L'Aquila, central Italy), Seismological Research Letters, 80(6), 940–950. https://doi.org/10.1785/gssrl.80.6.940

Faure Walker, J. P., G. P. Roberts, P. A. Cowie, I. D. Papanikolaou, P. R. Sammonds, A. M. Michetti, and R. J. Phillips (2009), Horizontal strain-rates and throw-rates across breached relay zones, central Italy: Implications for the preservation of throw deficits at points of normal fault linkage, J. Struct. Geol., 31(10), 1145–1160, doi:10.1016/j.jsg.2009.06.011.

Faure Walker, J. P., G. P. Roberts, P. R. Sammonds, and P. A. Cowie (2010), Comparison of earthquake strains over 10 2 and 10 4 year timescales: Insights into variability in the seismic cycle in the central Apennines, Italy, J. Geophys. Res., 115(B10), B10418, doi:10.1029/2009JB006462.

Faure Walker, J. P., G. P. Roberts, P. A. Cowie, I. Papanikolaou, A. M. Michetti, P. R. Sammonds, M. W. Wilkinson, K. McCaffrey and R. Phillips (2012), Relationship between topography, rates of extension and mantle dynamics in the actively-extending Italian Apennines, Earth and Planetary Science Letters 325-326, 76-84.

Ferrario, M. F., and F. Livio, (2018), Characterizing the Distributed Faulting During the 30 October 2016, Central Italy Earthquake: A Reference for Fault Displacement Hazard Assessment, Tectonics.

Field E. H., K. R. Milner, J. L. Hardebeck, M. T. Page, N. van der Elst, T. H. Jordan, A. J. Michael, B. E. Shaw and M. J. Werner (2017), A Spatiotemporal Clustering Model for the Third Uniform California Earthquake Rupture Forecast (UCERF3‐ETAS): Toward an Operational Earthquake Forecast, Bulletin of the Seismological Society of America, 107 (3): 1049–1081. doi: https://doi.org/10.1785/0120160173

Field E.H., G. P. Biasi, P. Bird, T. E. Dawson, K. R. Felzer, D. D. Jackson, K. M. Johnson, T. H. Jordan, C. Madden, A. J. Michael, K. R. Milner, M. T. Page, T. Parsons, P. M. Powers, B. E. Shaw, W. R. Thatcher, R. J. Weldon and Y. Zeng (2015), Long□Term Time□Dependent Probabilities for the Third Uniform California Earthquake Rupture Forecast (UCERF3), Bulletin of the Seismological Society of America, 105 (2A): 511–543. doi: https://doi.org/10.1785/0120140093

Field E. H., R. J. Arrowsmith, G. P. Biasi, P. Bird, T. E. Dawson, K. R. Felzer, D. D. Jackson, K. M. Johnson, T. H. Jordan, C. Madden, A. J. Michael, K. R. Milner, M. T. Page, T. Parsons, P. M. Powers, B. E. Shaw, W. R. Thatcher, R. J. Weldon ans Y. Zeng (2014), Uniform California Earthquake Rupture Forecast, Version 3 (UCERF3)—The Time□Independent Model. Bulletin of the Seismological Society of America, 104 (3): 1122–1180. doi: https://doi.org/10.1785/0120130164

Galadini, F., and P. Galli (2000), Active Tectonics in the Central Apennines (Italy)– Input Data for Seismic Hazard Assessment, Nat. Hazards, 22, 225–270.

Galli, P., F. Galadini, and D. Pantosti (2008), Twenty years of paleoseismology in Italy. Earth-Science Reviews, 88(1-2), pp.89-117.

Galli, P., B. Giaccio and P. Messina (2010), The 2009 central Italy earthquake seen through 0.5 Myr-long tectonic history of the L'Aquila faults system, Quaternary Science Reviews, 29(27-28), pp.3768-3789. https://doi.org/10.1016/j.quascirev.2010.08.018

Galli P. A. C., B. Giaccio, P. Messina, E. Peronace and G. M. Zuppi (2011), Palaeoseismology of the L'Aquila faults (central Italy, 2009, Mw 6.3 earthquake): implications for active fault linkage, Geophysical Journal International, Volume 187, Issue 3, Pages 1119–1134, https://doi.org/10.1111/j.1365-246X.2011.05233.x

Gori, S., E. Falcucci, S. Atzori, M. Chini, M. Moro, E. Serpelloni, G. Fubelli, M. Saroli, R. Devoti, S. Stramondo, F. Galadini, S. Salvi (2012), Constraining primary surface rupture length along the Paganica fault (L'Aquila earthquake) with geological and geodetic (DInSAR and GPS) evidence, Italian Journal of Geoscience, 131(3), 359–372. doi:10.3301/IJG.2012.21

Hampel, A., Li, T. and Maniatis, G., 2013. Contrasting strike-slip motions on thrust and normal faults: Implications for space-geodetic monitoring of surface deformation. Geology, 41(3), pp.299-302. DOI: 10.1130/G33927.1

Iezzi, F., Z. Mildon, J. F. Walker, G. Roberts, H. Goodall, M. Wilkinson, and J. Robertson (2018), Coseismic throw variation across along-strike bends on active normal faults: Implications for displacement versus length scaling of earthquake ruptures. Journal of Geophysical Research: Solid Earth, 123. https://doi.org/10.1029/2018JB016732

ISPRA (2009), Cartografia Geologica d'Italia 1:50,000 (Progetto CARG), sheet 359. http://www.isprambiente.gov.it/Media/carg/359_LAQUILA/Foglio.html

ISPRA (2009), Cartografia Geologica d'Italia 1:50,000 (Progetto CARG), sheet 349. http://www.isprambiente.gov.it/Media/carg/349_GRANSASSO/Foglio.html

Lavecchia, G., F. Ferrarini, F. Brozzetti, R. De Nardis, P. Boncio, and L. Chiaraluce, 2012. From surface geology to aftershock analysis: Constraints on the geometry of the L'Aquila 2009 seismogenic fault system. Italian Journal of Geosciences, 131(3), pp.330-347.

Livio, F., A. M. Michetti, E. Vittori, L. Gregory, L. Wedmore, L. Piccardi, E. Tondi, G. Roberts, A. M. Blumetti, L. Bonadeo, F. Brunamonte, and Central Italy Earthquake Working Group (2016), Surface faulting during the August 24, 2016, central Italy earthquake (Mw 6.0): preliminary results. Annals of geophysics, 59(Fast Track 5), pp.1-8, DOI: 10.4401/ag-7197

Ma, X.Q., and Kusznir, N.J., 1995, Coseismic and postseismic subsurface displacements and strains for a dip-slip normal fault in a three-layer elastic gravitational medium: Journal of Geophysical Research, v. 100, p. 12,813–12,828, doi:10.1029/95JB00674.

Manighetti, I., M. Campillo, S. Bouley, and F. Cotton (2007), Earthquake scaling, fault segmentation, and structural maturity. Earth and Planetary Science Letters, 253(3), 429-438.

Mildon, Z. K., G. P. Roberts, J. P. Faure Walker, L. Wedmore, and K. J. W. McCaffrey (2016), Active normal faulting during the 1997 seismic sequence in Colfiorito, Umbria: Did slip propagate to the surface?, J. Struct. Geol., doi:10.1016/j.jsg.2016.08.011.

Moro, M., S. Gori, E. Falcucci, M. Saroli, F. Galadini and S. Salvi (2013), Historical earthquakes and variable kinematic behaviour of the 2009 L'Aquila seismic event (central Italy) causative fault, revealed by paleoseismological investigations, Tectonophysics, 583, 131–144. http://dx.doi.org/10.1016/j.tecto.2012.10.036

Pace, B., L. Peruzza, G. Lavecchia, and P. Boncio (2006), Layered seismogenic source model and probabilistic seismic-hazard analyses in central Italy. Bulletin of the Seismological Society of America, 96(1), pp.107-132.

Papanikolaou, I.D., G. P. Roberts and A. M. Michetti (2005), Fault scarps and deformation rates in Lazio–Abruzzo, Central Italy: Comparison between geological fault slip-rate and GPS data. Tectonophysics, 408(1-4), pp.147-176. https://doi.org/10.1016/j.tecto.2005.05.043

Patacca, E., R. Sartori, and P. Scandone (1990), Tyrrhenian basin and Apenninic arcs: kinematic relations since late Tortonian times. Mem. Soc. Geol. It, 45(1), 425-451.

Pierantoni, P., G. Deiana, and S. Galdenzi (2013), Stratigraphic and structural features of the Sibillini Mountains (Umbria-Marche Apennines, Italy). Italian Journal of Geosciences, 132(3), 497-520. DOI: 10.3301/IJG.2013.08

Pizzi, A., and F. Galadini (2009), Pre-existing cross-structures and active fault segmentation in the northern-central Apennines (Italy), Tectonophysics, 476(1-2), 304-319. https://doi.org/10.1016/j.tecto.2009.03.018

Pizzi, A., and V. Scisciani (2000), Methods for determining the Pleistocene–Holocene component of displacement on active faults reactivating pre-Quaternary structures: examples from the central Apennines (Italy), Journal of Geodynamics 29, 29(3-5), pp.445-457. https://doi.org/10.1016/S0264-3707(99)00053-8

Pucci S., F. Villani, R. Civico, D. Pantosti, P. Del Carlo, A. Smedile, P. M. De Martini, E. Pons-Branchu and A. Gueli (2014): Quaternary geology of the Middle Aterno Valley, 2009 L'Aquila earthquake area (Abruzzi Apennines, Italy), Journal of Maps, DOI:10.1080/17445647.2014.927128

Roberts, G. P. (1996a), Noncharacteristic normal faulting surface ruptures from the Gulf of Corinth, Greece. Journal of Geophysical Research: Solid Earth, 101(B11), 25255-25267. 10.1029/96JB02119

Roberts, G. P. (1996b), Variation in fault-slip directions along active and segmented normal fault systems. Journal of Structural Geology, 18(6), 835-845.

Roberts, G.P. and Koukouvelas, I. (1996), Structural and seismological segmentation of the Gulf of Corinth fault system: implications for models of fault growth, Analli di Geofisica, 39, 619– 646.

Roberts, G.P. and Ganas, A. (2000), Fault□slip directions in central and southern Greece measured from striated and corrugated fault planes: Comparison with focal mechanism and geodetic data. Journal of Geophysical Research: Solid Earth, 105(B10), pp.23443-23462.

Roberts, G. P., A. M. Michetti, P. Cowie, N. C. Morewood, and I. Papanikolaou (2002), Fault slip□rate variations during crustal□scale strain localisation, central Italy, Geophysical Research Letters, 29(8). DOI: 10.1029/2001GL013529

Roberts, G. P., and A. M. Michetti (2004), Spatial and temporal variations in growth rates along active normal fault systems: an example from The Lazio–Abruzzo Apennines, central Italy. Journal of Structural Geology, 26(2), 339-376. http://dx.doi.org/10.1016/S0191-8141(03)00103-2

Roberts, G. P. (2007), Fault orientation variations along the strike of active normal fault systems in Italy and Greece: Implications for predicting the orientations of subseismic-resolution faults in hydrocarbon reservoirs. AAPG Bbulletin, 91(1), 1-20.

Roberts, G.P., B. Raithatha, G. Sileo, A. Pizzi, S. Pucci, J.F. Walker, M. Wilkinson, K. McCaffrey, R. J. Phillips, A. M. Michetti, and L. Guerrieri (2010), Shallow subsurface structure of the 2009 April 6 M w 6.3 L'Aquila earthquake surface rupture at Paganica, investigated with ground-penetrating radar, Geophysical Journal International, 183(2), pp.774-790. https://doi.org/10.1111/j.1365-246X.2010.04713.x

Tucker, G. E., S. W. McCoy, A. C. Whittaker, G. P. Roberts, S. T. Lancaster, and R. Phillips (2011), Geomorphic significance of postglacial bedrock scarps on normal-fault footwalls, J. Geophys. Res., 116, F01022, doi:10.1029/2010JF001861.

Vezzani, L., and F. Ghisetti (1998), Carta Geologica dell'Abruzzo, Scala 1:100,000. Firenze: S.EL.CA.

Villani, F., R. Civico, S. Pucci L. Pizzimenti, R. Nappi, P.M. De Martini and the Open EMERGEO Working Group (2018), A database of the coseismic effects following the 30 October 2016 Norcia earthquake in Central Italy, Scientific Data, doi: 10.1038/sdata.2018.49

Visini, F., A. Valentini, T. Chartier, O. Scotti and B. Pace (2019), Computational Tools for Relaxing the Fault Segmentation in Probabilistic Seismic Hazard Modelling in Complex Fault Systems, Pure and Applied Geophysics, 1-23, https://doi.org/10.1007/s00024-019-02114-6.

Vittori E., P. Di Manna, A. M. Blumetti, V. Comerci, L. Guerrieri, E. Esposito, A. M. Michetti, S. Porfido, L. Piccardi, G. P. Roberts, A. Berlusconi, F. Livio, G. Sileo, M. Wilkinson, K. J. W. McCaffrey, R. J. Phillips and P. A. Cowie (2011), Surface Faulting of the 6 April 2009 Mw 6.3 L'Aquila Earthquake in Central Italy. Bulletin of the Seismological Society of America, 101 (4): 1507–1530. doi: https://doi.org/10.1785/0120100140

Walters, R. J., J. R. Elliott, N. D'Agostino, P. C. England, I. Hunstad, J. A. Jackson, B. Parsons, R. J. Phillips, and G. Roberts (2009), The 2009 L'Aquila earthquake (central Italy): A source mechanism and implications for seismic hazard, Geophys. Res. Lett., 36, L17312, doi:10.1029/2009GL039337.

Wells, D. L., and K. J. Coppersmith (1994), New Empirical Relationships among Magnitude, Rupture Length, Rupture Width, Rupture Area, and Surface Displacement, Bull. Seismol. Soc. Am., 84(4), 974–1002.

Wesnousky, S.G. (2008), Displacement and Geometrical Characteristics of Earthquake Surface Ruptures: Issues and Implications for Seismic-Hazard Analysis and the Process of Earthquake Rupture, Bulletin of the Seismological Society of America 98, 1609–1632.

Wilkinson, M., G. P. Roberts, K. McCaffrey, P. A. Cowie, J. P. Faure Walker, I. Papanikolau, R. J. Phillips, A. M. Michetti, E. Vittori, L. Gregory, L. Wedmore, Z. K. Watson (2015), Slip distributions on active normal faults measured from LiDAR and field mapping of geomorphic offsets: an example from L'Aquila, Italy, and implications for modelling seismic moment release, Geomorphology, 237, 130–141, doi:10.1016/j.geomorph.2014.04.026.

Wilkinson, M., K. J. W. McCaffrey, G. Roberts, P. A. Cowie, R. J. Phillips, Alessandro Maria Michetti, E. Vittori, L. Guerrieri, A. M. Blumetti, A. Bubeck, and A. Yates (2010), Partitioned postseismic deformation associated with the 2009 Mw 6.3 L'Aquila earthquake surface rupture measured using a terrestrial laser scanner, Geophysical Research Letters, 37(10) DOI: 10.1029/2010GL043099

Figures caption

Figure 1 – Attributes of the 2016 M_w 6.0 and M_w 6.5 Mt. Vettore earthquakes, Central Italy. a) Partial and complete rupture of the Mt. Vettore fault during the 2016 seismic sequence. Two earthquakes have occurred on the same fault system, producing a partial (i; 24th August 2016 M_w 6.0 earthquake), and a complete rupture of the fault (ii; 30th October 2016 M_w 6.5 earthquake). Fault traces are adapted from Pierantoni et al. (2013). Digital elevation model is from Tarquini et al. (2012). Distribution of surface ruptures are adapted from Livio et al., 2016 for the 24th August 2016 M_w 6.0 earthquake and from Civico et al., 2018, and Villani et al., 2018, for the 30th October 2016 M_w 6.5 earthquake. b) Comparison between the i) geological throw, derived from geological cross-sections across pre-rift strata, the ii) coseismic throw following the 30th October M_w 6.5 earthquake (from Iezzi et al., 2018) and the iii) coseismic throw following the 24th August M_w 6.0 earthquake (from Iezzi et al., 2018) with the trace of the main Holocene fault scarp of the Mt. Vettore fault (panel iv)). Both coseismic throws and geological throw profiles are asymmetric, with maxima values across an along-strike fault bend within the main Holocene fault trace of the Mt. Vettore fault,

which is identified by the construction of strike lines (in red in panel iv). (modified from Iezzi et al., 2018).

Figure 2 – Location map of the Aterno Valley Fault System, central Apennines, Italy. Thick red lines are normal fault segments part of the Aterno Valley Fault System, thin red lines are other active normal faults part of the Central Apennines Fault System. Black lines are traces of the geological cross sections. Black triangles are locations of measurements of post 15±3 ka fault throw obtained from fault scarp measurements (from Roberts and Michetti, 2004; Papanikolaou et al., 2005; Galli et al., 2011; our own fieldwork); blue triangles are locations of measurements of post 15±3 ka fault throw derived from throw rates obtained with palaeoseismological analysis, assuming these throw rates constant within the last 15±3 ka (from Galli et al., 2010; 2011; Cinti et al., 2011). Red stars are the epicentres of the 6th April 2009 M_w 6.3 L'Aquila earthquake mainshock and of the 7th April 2009 M_w 5.6 aftershock. Pale blue lines are the traces of the coseismic surface ruptures following the 6th April 2009 M_w 6.3 L'Aquila earthquake (modified from Vittori et al., 2011). Blue and pink dashed lines define the areas of subsidence and uplift, respectively, derived from DiNSAR analysis (Papanikolaou et al., 2010). a-a' and b-b' are traces of profiles across the deformed areas (see Figure 9). Yellow lines are topographic profiles used to derive the topographic relief associated with the Aterno Valley Fault System (showed in Figure 9c).

Figure 3 – Coseismic ruptures following the 2009 L'Aquila earthquake. a) Coseismic scarp in eluvial-colluvial deposits, with vertical offset of ~10 cm. b) Opening cracks on the ground surface. c) Surface rupture on concrete, with vertical offset of ~10 cm. d) Location map of the surface ruptures showed in a), b) and c).

Figure 4– Palaeoseismological hypothesis of the occurrence of multi-fault earthquakes across the Aterno Valley Fault System. (a) shows in blue fault segments inferred to have ruptured during the 1703 M_w 6.7 earthquake, following Galli et al., 2011. Yellow polygons are locations of palaeoseismological studies with evidences of rupture ascribable to the 1703 earthquake (from Galli et al., 2011). (b) shows in blue surface ruptures following the 6th April 2009 M_w 6.3 earthquake, modified after Vittori et al., 2011. It is shown that palaeoseismological studies suggest that the 1703 M_w 6.7 earthquake have ruptured at the same time several fault segments across the total extension of the fault system, suggesting the occurrence of multi-fault earthquakes.

Figures 5 –Geological cross-sections built across the Aterno valley fault system. (a) Geological map of the Aterno Valley Fault System, modified from Vezzani and Ghisetti, 1998. In red are faults part of the Aterno Valley Fault System, in black traces of the cross-sections. The stratigraphy is derived from Vezzani and Ghiseeti, 1998, map; colours are in agreement with the ones reported in the map, and used in the cross-sections to highlight the offset on fault. Here are shown cross-sections from 1 to 13. b) Cross-sections from 14 to 39. BRF: Barisciano fault; PSDF: Paganica-San Demetrio fault; BTF: Barete fault; PF: Pettino fault. When it was not possible to establish the thickness of a formation, we assigned it the maximum thickness provided by the legend of the map.

Figure 6 – Location map of the fault scarps and palaeoseismological studies used to constrain the throw rates since the demise of the Last Glacial Maximum (15±3 ka) along the Aterno Valley Fault System, comprehensive of published and newly collected data. Location numbers are coded in agreement with the name of the fault to which they belong:

BRF=Barisciano fault; PSDF=Paganica-San Demetrio fault; PF=Pettino fault; BTF=Barete fault.

Figure 7 – Newly collected field measurements of throw and throw-rates since the demise of the Last Glacial Maximum (15±3 ka) from fault scarps located along the Aterno Valley Fault System. a) Interpreted scarp profiles showing the measured throw associated with the fault scarp. Scarp profiles have been built through chain surveying techniques using a 1 m ruler and a clinometer. Location numbers are coded in agreement with the database shown in Figure 6b. b) Location map of the field locations in a). c) Sketch of a fault scarp to show the criteria we have followed to select the site of measurement. Measurements of scarp height are collected only in locations where upper and lower slopes and hangingwall and footwall cut-offs are preserved since the demise of the LGM (15±3 ka), so to represent the throw accumulated during the last 15±3 ka.

Figure 8 – Analysis of the geometry of the Aterno Valley Fault System. In black are reported strike lines built on the main fault segments of the fault system. Strike lines are lines joining locations at the same elevation, and therefore they provide a good representation of the overall strike of the fault segments. It is shown that the fault system presents a wide along-strike bend, across which the strike of different fault segments changes, with an overall shift of ~25º from the strike of the fault segments outside the fault bend (outer faults).

Figure 9 – Throw profiles of the Aterno Valley Fault System. a) Long-term throw profiles of the main faults of the fault system. Values of throw are derived from geological cross-sections shown in Figures 5a-5b. In blue is reported the cumulative throw profile of the fault system, calculated by summing up the throw values across each fault segment. b) Profiles of

the throw accumulated since the demise of the Last Glacial Maximum (15±3 ka) across the fault system. Squares are values of throw derived from fault scarp measurements (Roberts and Michetti, 2004; Papanikolaou et al., 2005; Galli et al., 2011; our own fieldwork), triangles are values of throw derived from palaeoseismological analysis (palaeoseismological throw rate times 15±3 ka; Galli et al., 2010; 2011; Cinti et al., 2011). In blue is the cumulative LGM throw profile of the entire fault system. Throw rates, reported on the left-hand side, are calculated assuming a constant throw rate within the last 15ka. c) Topographic relief associated with the footwall escarpment of the Aterno Valley Fault System. In orange is the topographic profile of the footwall, in blue of the hangingwall, derived from 10m DEM. d) Profiles of coseismic deformation areas of uplift and subsidence following the 6^{th} April 2009 M_w 6.3 mainshock and the 7^{th} April 2009 M_w 5.6 aftershock, derived from DInSAR analysis (profile traces a-a' and b-b' in Figure 2; adapted from Papanikolaou et al., 2010). e) Along-strike profiles of the coseismic slip of the 6^{th} April 2009 M_w 6.3 L'Aquila earthquake, derived from different geodetic and seismological fault models (Atzori et al., 2009; Walters et al., 2009; Cheloni et al., 2010; Cirella et al., 2010; D'Agostino et al., 2012). Profiles have been drawn at 7.5 km depth. f) Reconstruction of the segmentation of the principal faults forming the Aterno Valley Fault System. This figure shows that 1) the 2009 earthquake ruptured only a small part of a complex fault system, 2) faults within the Aterno Valley Fault System are interacting over several earthquake cycles, with potential to release multi-fault earthquakes, 3) maximum throws are localized within a fault bend, which is a persistent feature influencing the throw distribution over the history of the fault system.

Figure 10 – Comparison between the measured long-term throw profile (blue line) and the predicted long-term throw profile (red line), assuming constant post-LGM throw rates during the last 3 Ma. It shows that the two profiles are overall consistent, which suggest that the

post-LGM throw rates can be representative of the throw rates averaged over the entire faults activity. Local discrepancies prompt the idea that post-LGM throw rates are working in order to produce a throw profile which reflect the long-term throw profile.

Figure 11 – Complete and partial ruptures of the Aterno Valley Fault System. a) Fault map of the Aterno Valley Fault System showing that it can experience complete ruptures, involving all its fault segments (red bar), and partial ruptures, as is the case of the 2009 M_w 6.3 L'Aquila earthquake (green bar). b) Moment Magnitude versus Surface Rupture Length scaling relationship (Wells and Coppersmith, 1994), with reported partial and total ruptures of the Aterno Valley Fault System.

Table Caption

Table 1 – Database of measurements of throw and throw rates showed in Figure 6 and 7.

Fault name	X UTM value	Y UTM value	Location number	Throw value (m)	Throw rate (mm/yr)	Technique used to constrain throw-rate	Notes on geomorphic features and palaeoseismological sites used to derive throw rates	References
Barisciano	392297	4679320	BRF1	6.1	0.4	Fault scarp profile	Bedrock fault scarp. Offset of slope but no Quaternary sediments on scarp.	New measurement
	391907	4679658	BRF2	7	0.4	Fault scarp profile	Two profiles within 80 m provided max (7m) and min (4.4m) throws. The mean throw rate is 0.032±0.07 mm/yr. In this paper we have considered the maximum measured throw and throw rate.	Loc. 20 Papanikolaou et al. 2005
	391951	4679798	BRF3	5	0.3	Fault scarp profile	Bedrock fault scarp. Offset of slope but no Quaternary sediments on scarp.	Loc. 21 Roberts and Michetti 2004
	384225	4687552	BRF4	3.5	0.2	Fault scarp profile	Throw estimated by eye across an antithetic scarp. Cultivation processes heavily disturbed the locality.	Loc. 18 Papanikolaou et al. 2005
	383475	4689190	BRF5	6.5	0.4	Fault scarp profile	Bedrock fault scarp. Offset of slope but no Quaternary sediments on scarp.	New measurement
	383457	4689203	BRF6	7	0.4	Fault scarp profile	Main bedrock scarp dipping SW, with 3-4 m high free face.	Loc. 16 Papanikolaou et al. 2005
	383561	4689552	BRF7	6.5	0.4	Fault scarp profile	The value of throw and throw-rate used in this paper is the one of the main SW-dipping fault at this locality.	Loc. 22 Roberts and Michetti 2004
	369075	4698110	BRF8	7	0.4	Fault scarp profile	Bedrock fault scarp. Offset of slope but no Quaternary sediments on scarp.	New measurement
	368500	4698400	BRF9	3	0.2	Fault scarp profile	Large striated fault surface. Maximum assumed rate.	Loc. 23 Roberts and Michetti 2004
Paganica-San Demetrio	374988	4690469	PSDF1	3.75	0.25	Palaeoseismological trench	Slip-rate for the last 2.5 kyrs. In this paper it has been assumed constant during the last 15kyr.	Trench1 Galli et al. 2010
	374615	4690589	PSDF2	4.5	0.3	Palaeoseismological trench	Late Pleistocene slip-rate, assumed constant during the last 15kyr.	Loc. Tret Cinti et al. 2011
	374007	4691381	PSDF3	4.95	0.33	Palaeoseismological trench	Slip-rate for the last 2.5 kyrs. In this paper it has been assumed constant during the last 15kyr.	Trench2 Galli et al. 2010
	373904	4691470	PSDF4	6	0.4	Palaeoseismological trench	Late Pleistocene slip-rate, assumed constant during the last 15kyr.	Loc. Acq Cinti et al. 2011
	371915	4694556	PSDF5	4.5	0.3	Fault scarp profile	Bedrock fault scarp. Offset of slope but no Quaternary sediments on scarp.	New measurement
Pettino	365551	4692675	PF1	10	0.6	Fault scarp profile	Post-LGM throw and throw-rate measured on basal fault scarp.	Loc. T3 Galli et al. 2011
Barete	361561	4699376	BTF1	10.5	0.7	Fault scarp profile	Throw-rate constrained measuring vertical offset of dated Quaternary deposits (Galadini and Galli, 2000) along basal fault scarp.	Loc.T1 Galli et al. 2011
	362067	4699769	BTF2	6	0.4	Fault scarp profile	Degraded fault scarp.	Loc. 33 Roberts and Michetti 2004
	360138	4700170	BTF3	10.5	0.7	Fault scarp profile	Throw-rate constrained measuring vertical offset of dated Quaternary deposits (Galadini and Galli, 2000) along basal fault scarp.	Loc.1 Galli et al. 2011
	361337	4700476	BTF4	8.5	0.5	Fault scarp profile	Bedrock scarp height of 7 - 10 m. Slope offset but no Quaternary deposits noted.	Loc. 34 Roberts and Michetti 2004
	358438	4702072	BTF5	9.1	0.5	Fault scarp profile	Bedrock fault scarp with 7 m free face.	Loc. 24 Papanikolaou et al. 2005
	357725	4703268	BTF6	11.5	0.7	Fault scarp profile	Bedrock fault scarp. Offset of slope but no Quaternary sediments on scarp.	New measurement
	354574	4706216	BTF7	4.5	0.3	Fault scarp profile	Disturbed fault scarp due to town built on scarp. The throw-rate used herein is probably the maximum for the location.	Loc. 35 Roberts and Michetti 2004

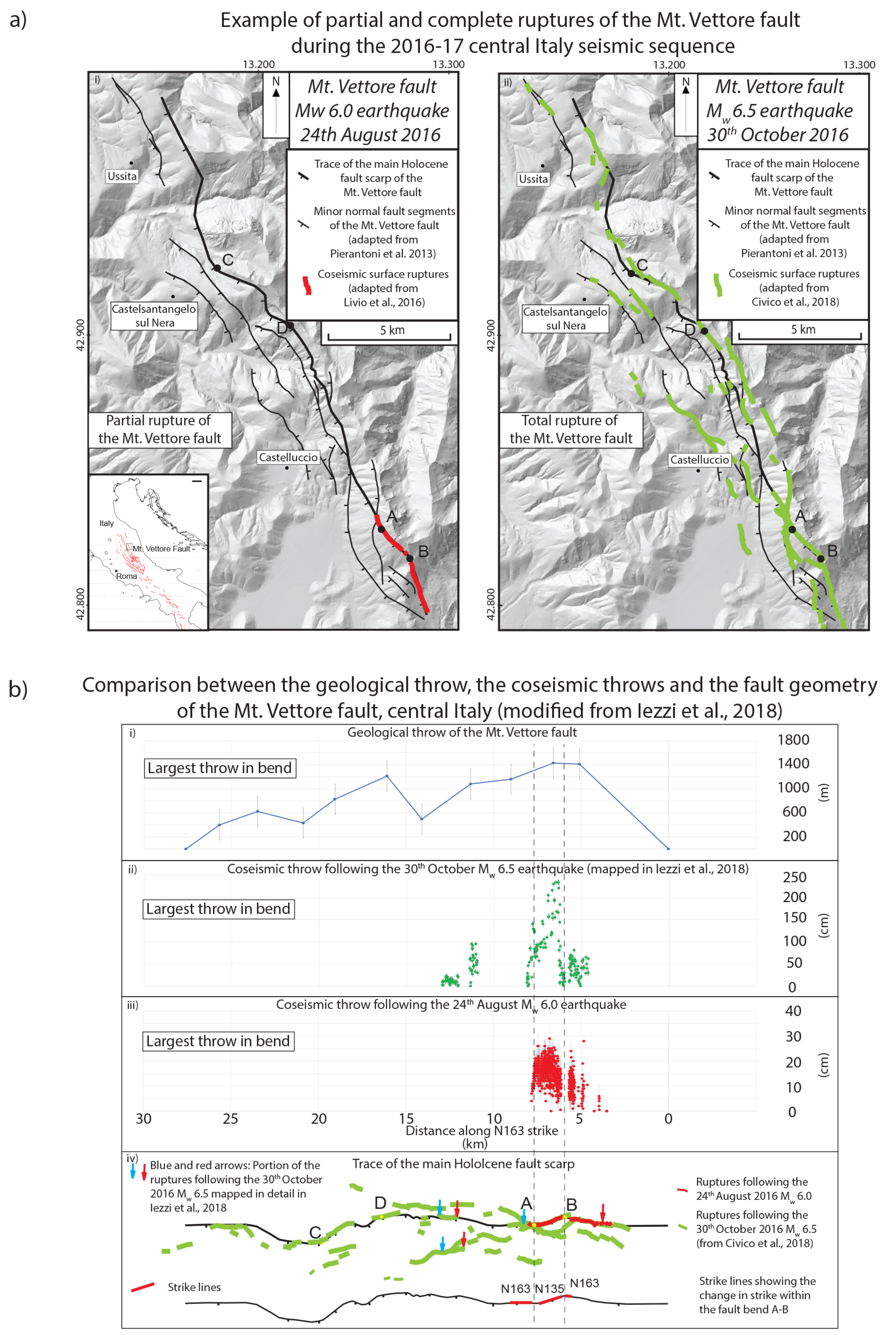
a)
Example of partial and complete ruptures of the Mt. Vettore fault
during the 2016-17 central Italy seismic sequence
13.200
13.300
i)
Mt. Vettore fault
Mw 6.0 earthquake
24th August 2016
Trace of the main Holocene fault scarp of the Mt. Vettore fault
Minor normal fault segments of the Mt. Vettore fault (adapted from Pierantoni et al. 2013)
Coseismic surface ruptures (adapted from Livio et al., 2016)
5 km
Ussita
Castelsantangelo sul Nera
Castelluccio
Partial rupture of the Mt. Vettore fault
42.900
42.800
Italy
Mt. Vettore Fault
Roma
ii)
Mt. Vettore fault
Mw 6.5 earthquake
30th October 2016
Coseismic surface ruptures (adapted from Civico et al., 2018)
Total rupture of the Mt. Vettore fault
b)
Comparison between the geological throw, the coseismic throws and the fault geometry
of the Mt. Vettore fault, central Italy (modified from Iezzi et al., 2018)
i)
Geological throw of the Mt. Vettore fault
Largest throw in bend
1800
1400
1000
600
200
(m)
ii)
Coseismic throw following the 30th October Mw 6.5 earthquake (mapped in Iezzi et al., 2018)
Largest throw in bend
250
200
150
100
50
0
(cm)
iii)
Coseismic throw following the 24th August Mw 6.0 earthquake
Largest throw in bend
40
30
20
10
0
(cm)
30
25
20
15
10
5
0
Distance along N163 strike (km)
iv)
Blue and red arrows: Portion of the ruptures following the 30th October 2016 Mw 6.5 mapped in detail in Iezzi et al., 2018
Trace of the main Hololcene fault scarp
Ruptures following the 24th August 2016 Mw 6.0
Ruptures following the 30th October 2016 Mw 6.5 (from Civico et al., 2018)
A
B
C
D
Strike lines
N163
N135
N163
Strike lines showing the change in strike within the fault bend A-B

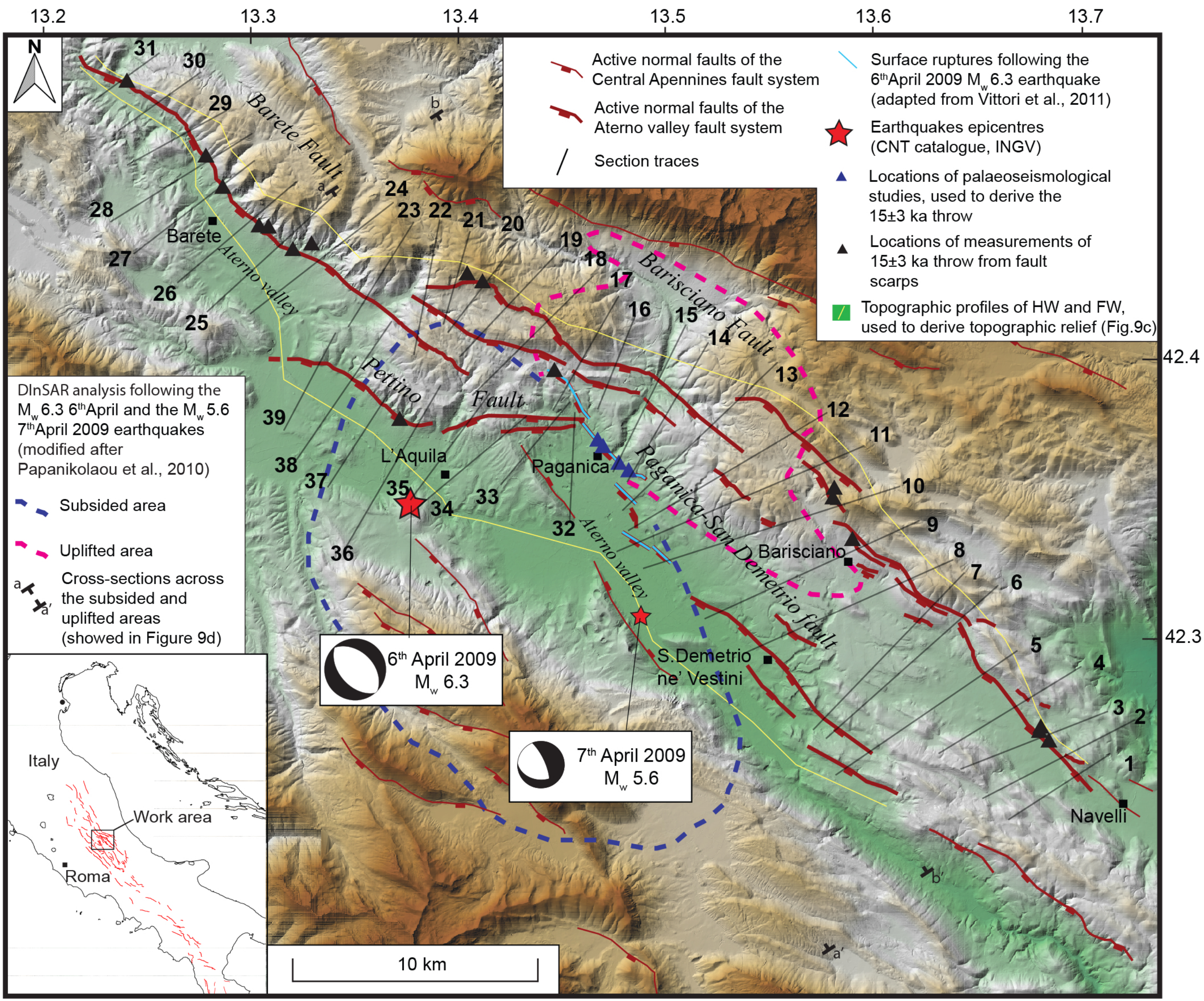
13.2
13.3
13.4
13.5
13.6
13.7
42.4
42.3
N
Active normal faults of the Central Apennines fault system
Active normal faults of the Aterno valley fault system
Section traces
Surface ruptures following the 6th April 2009 Mw 6.3 earthquake (adapted from Vittori et al., 2011)
Earthquakes epicentres (CNT catalogue, INGV)
Locations of palaeoseismological studies, used to derive the 15±3 ka throw
Locations of measurements of 15±3 ka throw from fault scarps
Topographic profiles of HW and FW, used to derive topographic relief (Fig.9c)
DInSAR analysis following the Mw 6.3 6thApril and the Mw 5.6 7thApril 2009 earthquakes (modified after Papanikolaou et al., 2010)
Subsided area
Uplifted area
Cross-sections across the subsided and uplifted areas (showed in Figure 9d)
Barete Fault
Barete
Aterno valley
Pettino Fault
Barisciano Fault
Paganica-San Demetrio fault
L'Aquila
Paganica
Bariscianо
S.Demetrio ne' Vestini
Navelli
6th April 2009 Mw 6.3
7th April 2009 Mw 5.6
Italy
Work area
Roma
10 km
a
a'
b
b'
1
2
3
4
5
6
7
8
9
10
11
12
13
14
15
16
17
18
19
20
21
22
23
24
25
26
27
28
29
30
31
32
33
34
35
36
37
38
39

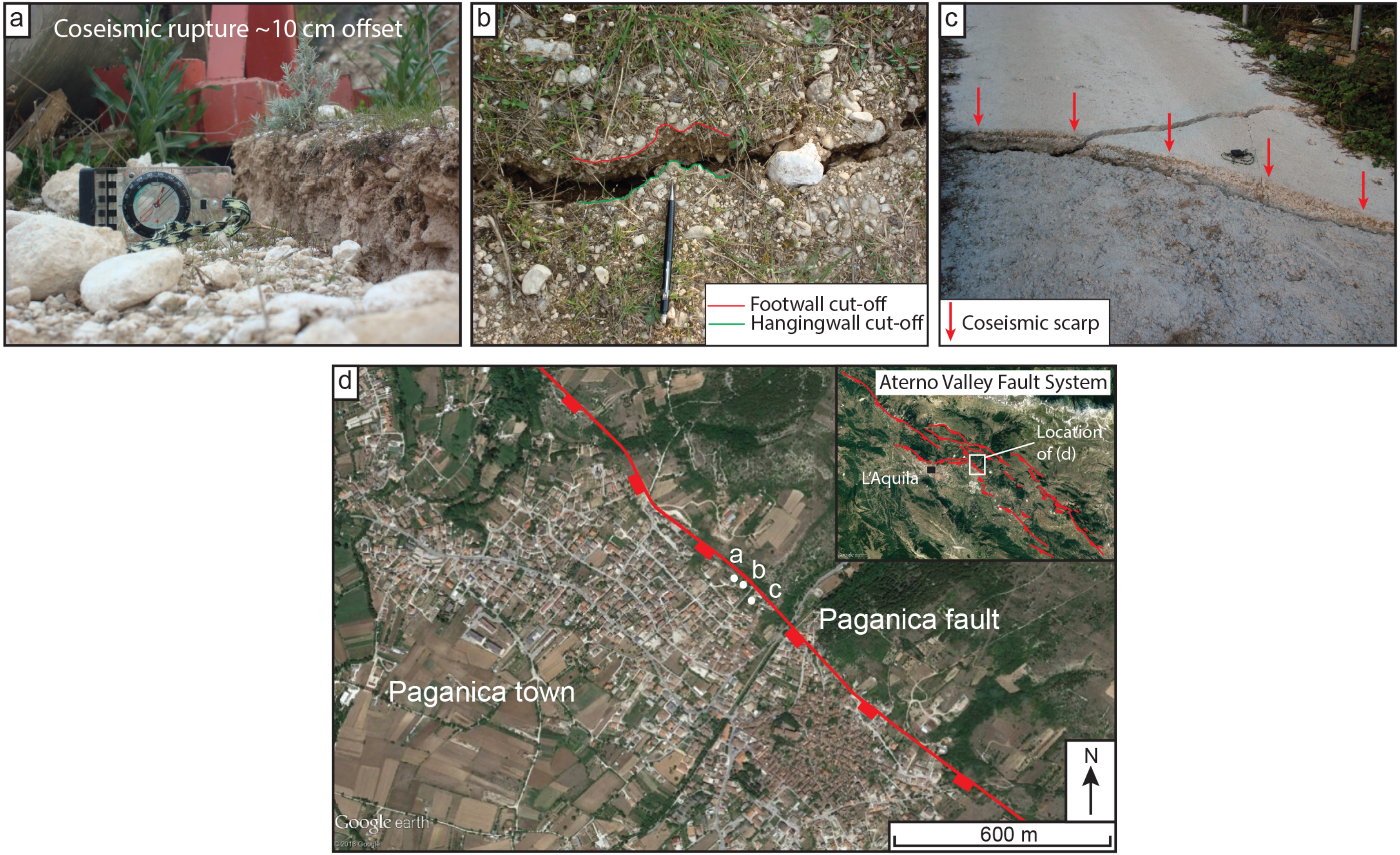
a
Coseismic rupture ~10 cm offset
b
Footwall cut-off
Hangingwall cut-off
c
Coseismic scarp
d
Aterno Valley Fault System
Location of (d)
L'Aquila
a
b
c
Paganica fault
Paganica town
N
600 m
Google earth

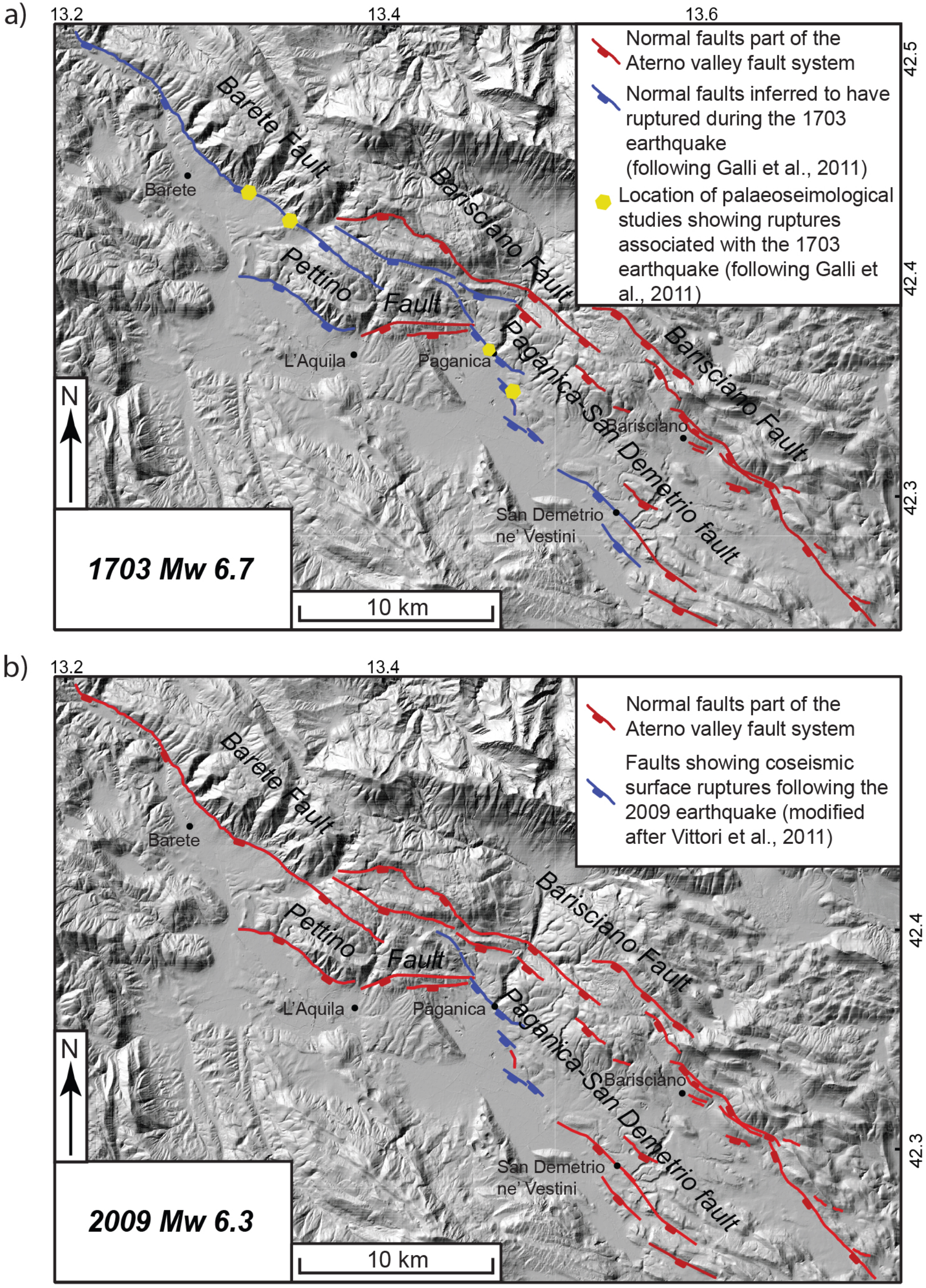
a)
13.2
13.4
13.6
42.5
42.4
42.3
Normal faults part of the Aterno valley fault system
Normal faults inferred to have ruptured during the 1703 earthquake (following Galli et al., 2011)
Location of palaeoseimological studies showing ruptures associated with the 1703 earthquake (following Galli et al., 2011)
Barete Fault
Barete
Barisciano Fault
Pettino Fault
L'Aquila
Paganica
Paganica-San Demetrio fault
Barisciano
San Demetrio ne' Vestini
N
1703 Mw 6.7
10 km
b)
13.2
13.4
42.4
42.3
Normal faults part of the Aterno valley fault system
Faults showing coseismic surface ruptures following the 2009 earthquake (modified after Vittori et al., 2011)
Barete Fault
Barete
Barisciano Fault
Pettino Fault
L'Aquila
Paganica
Paganica-San Demetrio fault
Barisciano
San Demetrio ne' Vestini
N
2009 Mw 6.3
10 km

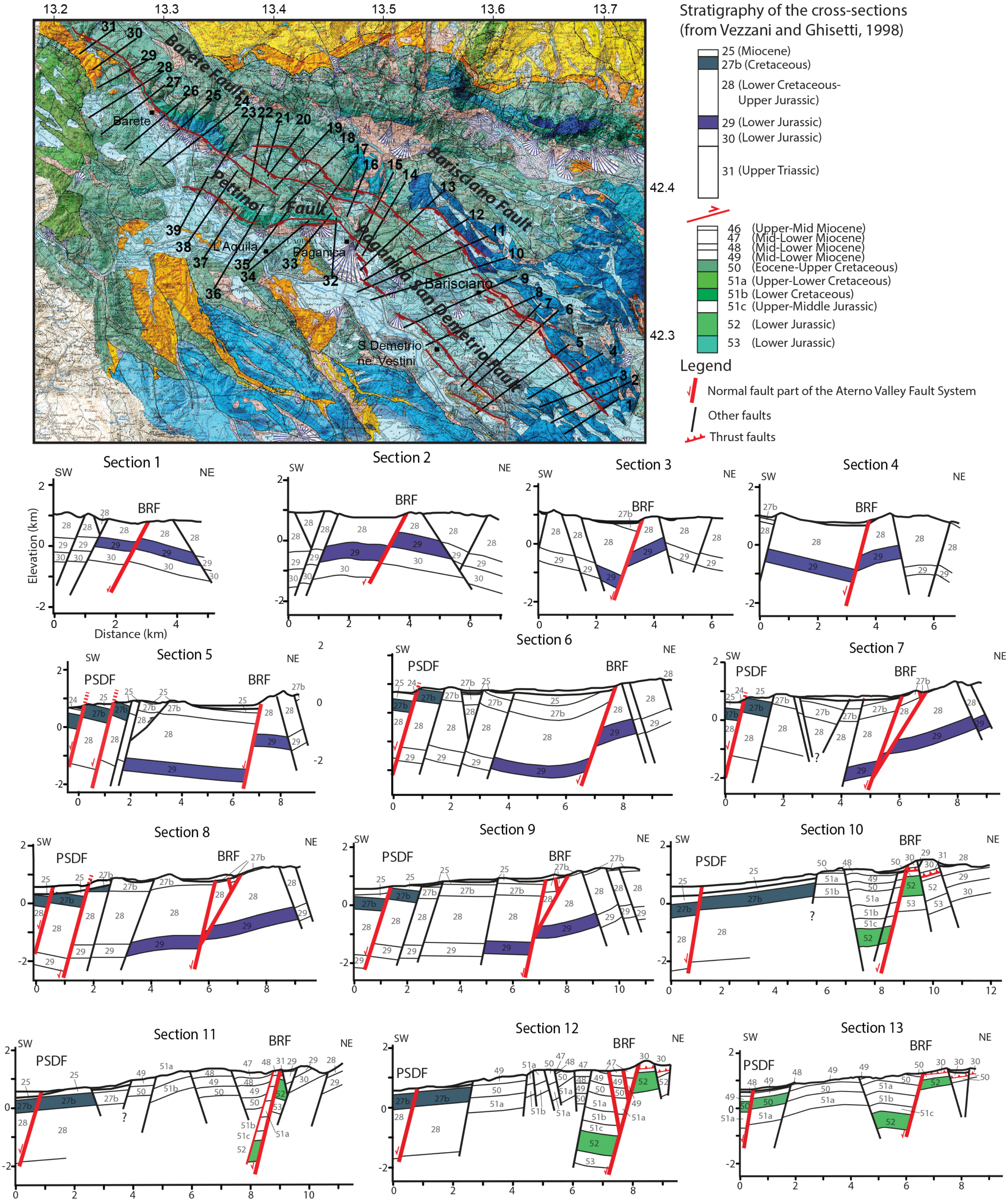

13.2
13.3
13.4
13.5
13.6
13.7
42.4
42.3
Barete Fault
Pettino Fault
Bariscisano Fault
Paganica San Demetrio Fault
Barete
L'Aquila
Paganica
Barisciano
S.Demetrio ne' Vestini
Stratigraphy of the cross-sections (from Vezzani and Ghisetti, 1998)
25 (Miocene)
27b (Cretaceous)
28 (Lower Cretaceous-Upper Jurassic)
29 (Lower Jurassic)
30 (Lower Jurassic)
31 (Upper Triassic)
46 (Upper-Mid Miocene)
47 (Mid-Lower Miocene)
48 (Mid-Lower Miocene)
49 (Mid-Lower Miocene)
50 (Eocene-Upper Cretaceous)
51a (Upper-Lower Cretaceous)
51b (Lower Cretaceous)
51c (Upper-Middle Jurassic)
52 (Lower Jurassic)
53 (Lower Jurassic)
Legend
Normal fault part of the Aterno Valley Fault System
Other faults
Thrust faults
Section 1
Section 2
Section 3
Section 4
Section 5
Section 6
Section 7
Section 8
Section 9
Section 10
Section 11
Section 12
Section 13
SW
NE
BRF
PSDF
Elevation (km)
Distance (km)

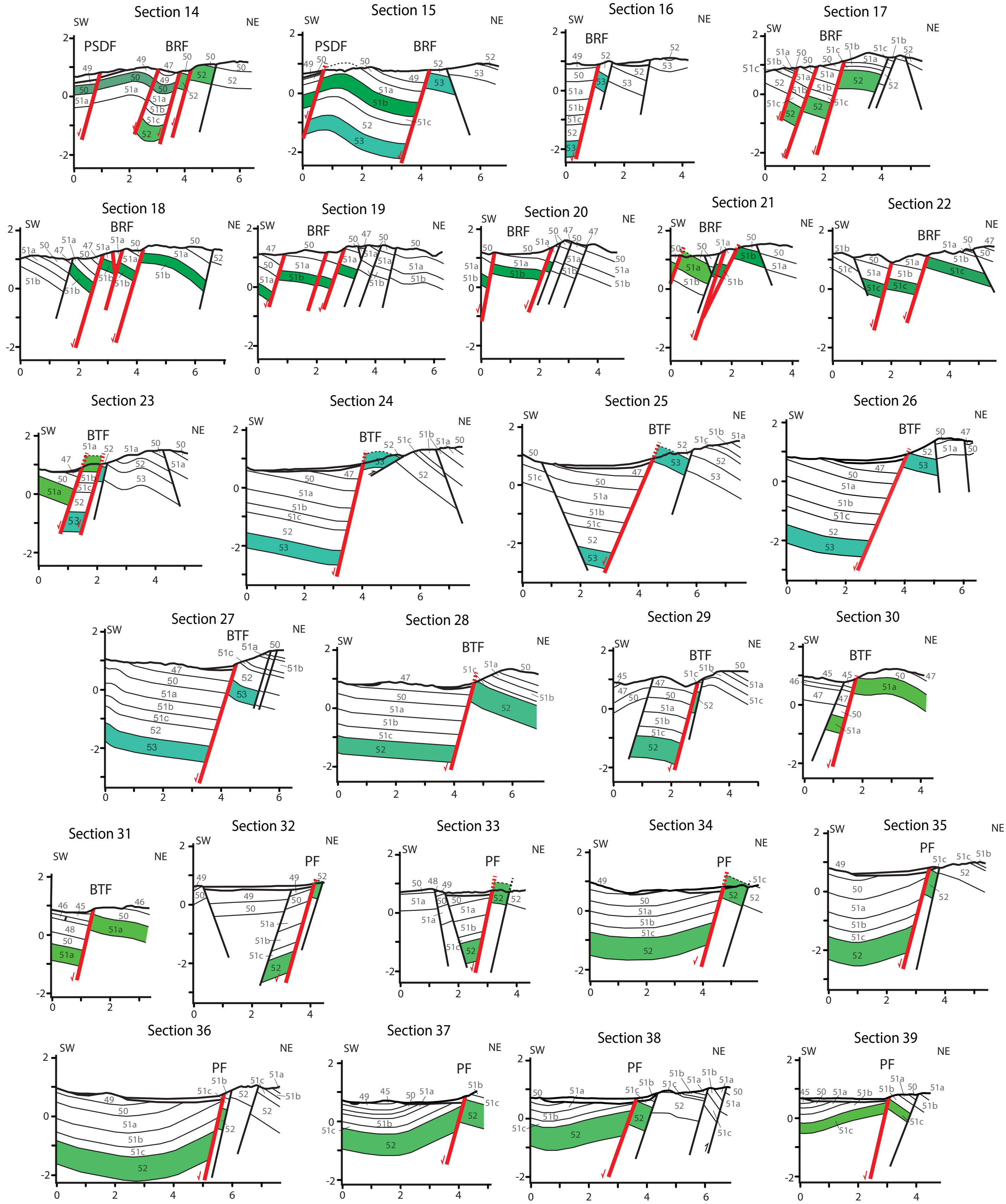
Section 14
SW
NE
PSDF
BRF
Section 15
PSDF
BRF
Section 16
BRF
Section 17
BRF
Section 18
BRF
Section 19
BRF
Section 20
BRF
Section 21
BRF
Section 22
BRF
Section 23
BTF
Section 24
BTF
Section 25
BTF
Section 26
BTF
Section 27
BTF
Section 28
BTF
Section 29
BTF
Section 30
BTF
Section 31
BTF
Section 32
PF
Section 33
PF
Section 34
PF
Section 35
PF
Section 36
PF
Section 37
PF
Section 38
PF
Section 39
PF

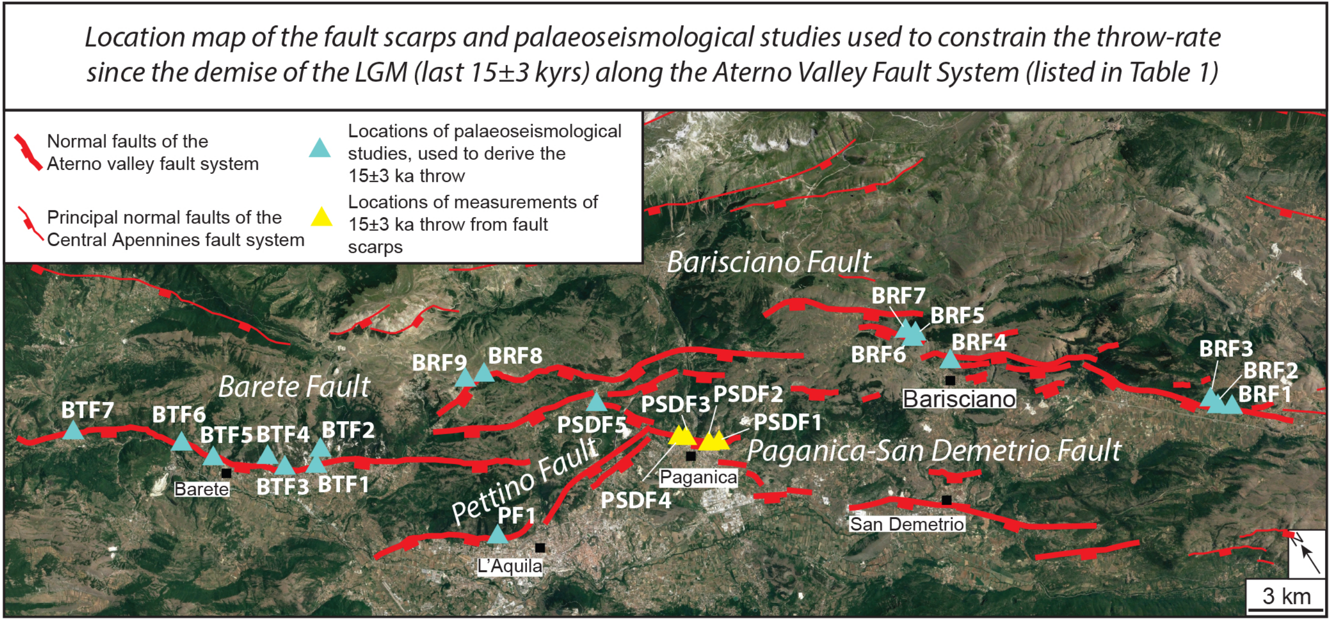
Location map of the fault scarps and palaeoseismological studies used to constrain the throw-rate since the demise of the LGM (last 15±3 kyrs) along the Aterno Valley Fault System (listed in Table 1)
Normal faults of the Aterno valley fault system
Principal normal faults of the Central Apennines fault system
Locations of palaeoseismological studies, used to derive the 15±3 ka throw
Locations of measurements of 15±3 ka throw from fault scarps
Barisciano Fault
Barete Fault
Pettino Fault
Paganica-San Demetrio Fault
BRF7
BRF5
BRF4
BRF6
BRF3
BRF2
BRF1
BRF9
BRF8
BTF7
BTF6
BTF5
BTF4
BTF2
BTF3
BTF1
PSDF5
PSDF3
PSDF2
PSDF1
PSDF4
PF1
Barisciano
Barete
Paganica
San Demetrio
L'Aquila
3 km

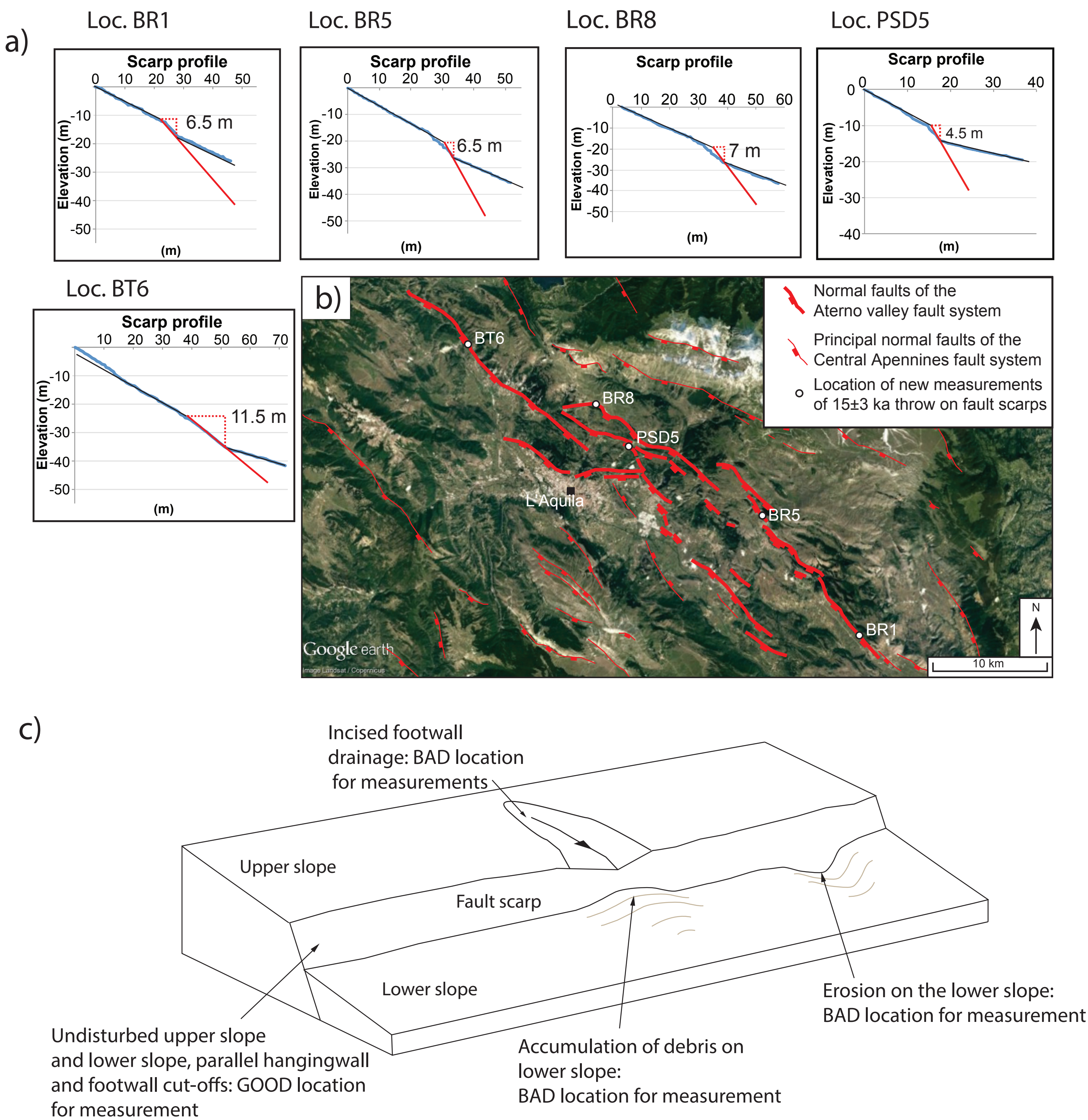
a)
Loc. BR1
Scarp profile
6.5 m
Elevation (m)
(m)
Loc. BR5
Scarp profile
6.5 m
Elevation (m)
(m)
Loc. BR8
Scarp profile
7 m
Elevation (m)
(m)
Loc. PSD5
Scarp profile
4.5 m
Elevation (m)
(m)
Loc. BT6
Scarp profile
11.5 m
Elevation (m)
(m)
b)
Normal faults of the Aterno valley fault system
Principal normal faults of the Central Apennines fault system
Location of new measurements of 15±3 ka throw on fault scarps
BT6
BR8
PSD5
L'Aquila
BR5
BR1
N
10 km
Google earth
c)
Incised footwall drainage: BAD location for measurements
Upper slope
Fault scarp
Lower slope
Undisturbed upper slope and lower slope, parallel hangingwall and footwall cut-offs: GOOD location for measurement
Accumulation of debris on lower slope: BAD location for measurement
Erosion on the lower slope: BAD location for measurement

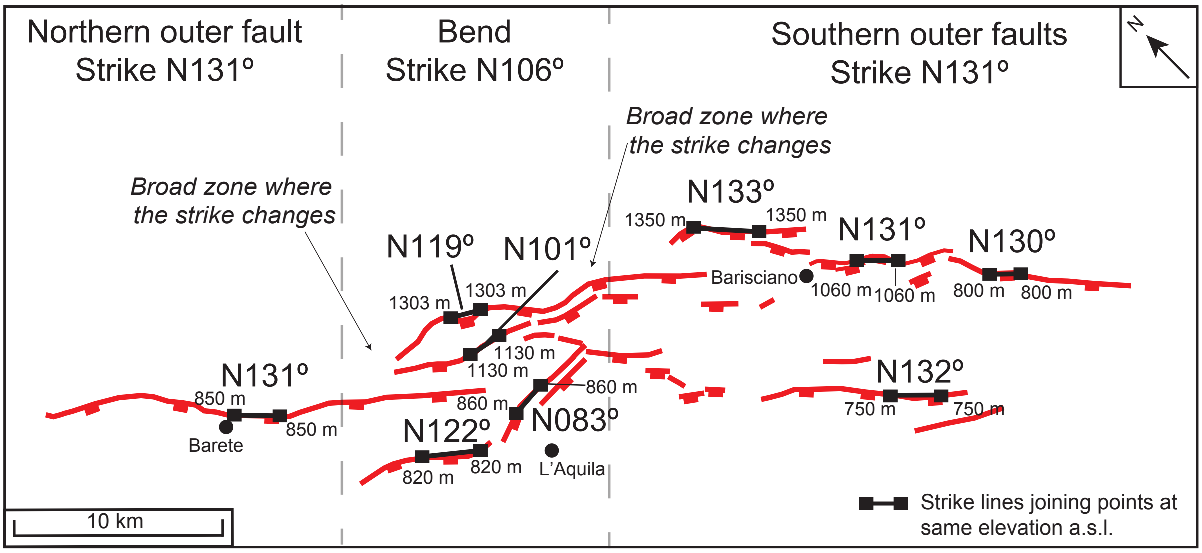

Northern outer fault
Strike N131°
Bend
Strike N106°
Southern outer faults
Strike N131°
N
Broad zone where the strike changes
Broad zone where the strike changes
N133°
1350 m
1350 m
N131°
N130°
N119°
N101°
1303 m
1303 m
Barisciano
1060 m
1060 m
800 m
800 m
1130 m
1130 m
N131°
850 m
850 m
Barete
860 m
860 m
N083°
N132°
750 m
750 m
N122°
820 m
820 m
L'Aquila
10 km
Strike lines joining points at same elevation a.s.l.

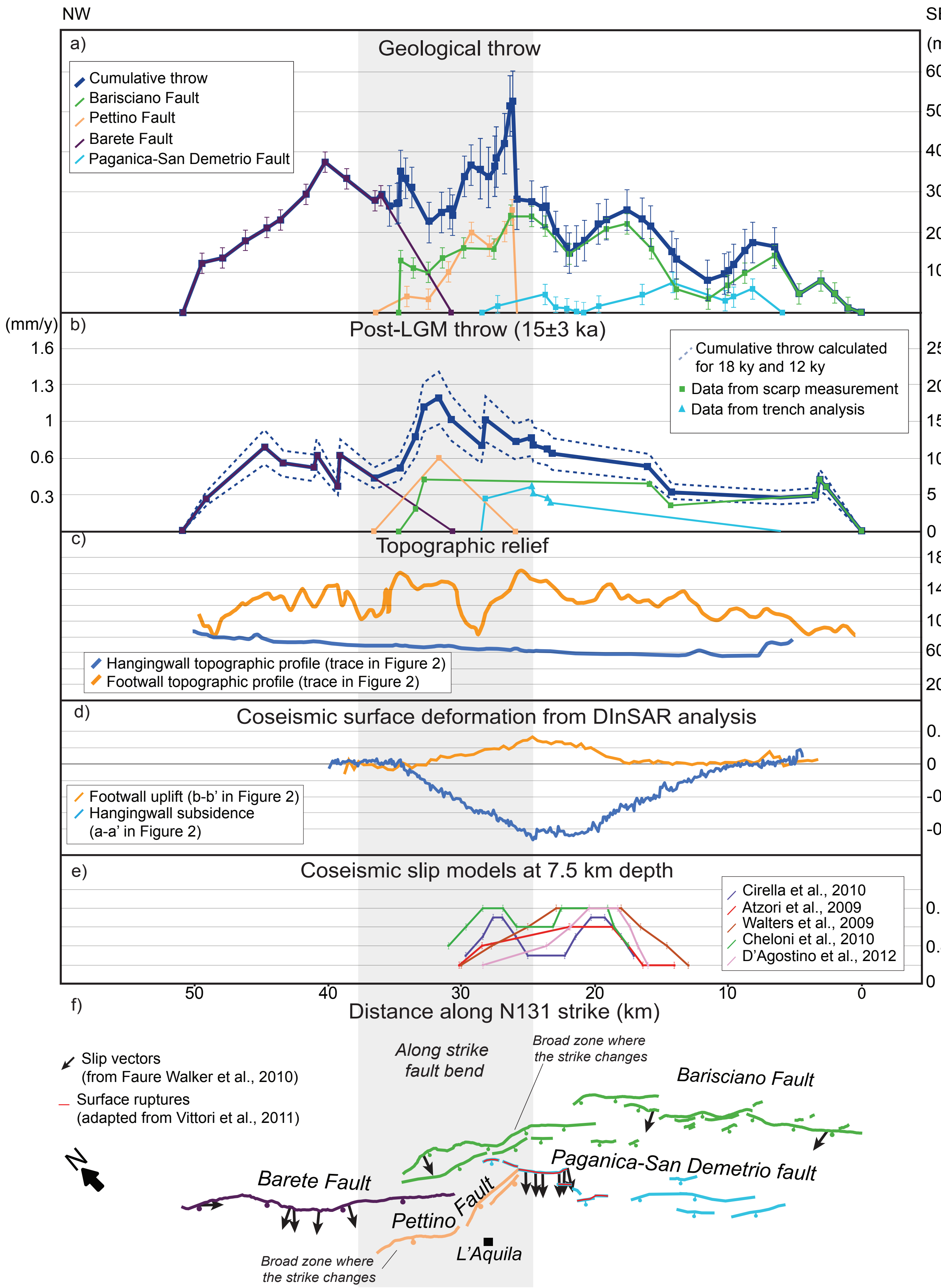
NW
SE
a)
Geological throw
(m)
6000
5000
4000
3000
2000
1000
Cumulative throw
Barisciano Fault
Pettino Fault
Barete Fault
Paganica-San Demetrio Fault
(mm/y)
b)
Post-LGM throw (15±3 ka)
1.6
1.3
1
0.6
0.3
25
20
15
10
5
0
Cumulative throw calculated for 18 ky and 12 ky
Data from scarp measurement
Data from trench analysis
c)
Topographic relief
1800
1400
1000
600
200
Hangingwall topographic profile (trace in Figure 2)
Footwall topographic profile (trace in Figure 2)
d)
Coseismic surface deformation from DInSAR analysis
0.10
0
-0.10
-0.20
Footwall uplift (b-b' in Figure 2)
Hangingwall subsidence (a-a' in Figure 2)
e)
Coseismic slip models at 7.5 km depth
Cirella et al., 2010
Atzori et al., 2009
Walters et al., 2009
Cheloni et al., 2010
D'Agostino et al., 2012
0.8
0.4
0
50
40
30
20
10
0
f)
Distance along N131 strike (km)
Slip vectors (from Faure Walker et al., 2010)
Surface ruptures (adapted from Vittori et al., 2011)
N
Along strike fault bend
Broad zone where the strike changes
Barisciano Fault
Paganica-San Demetrio fault
Barete Fault
Pettino Fault
L'Aquila
Broad zone where the strike changes

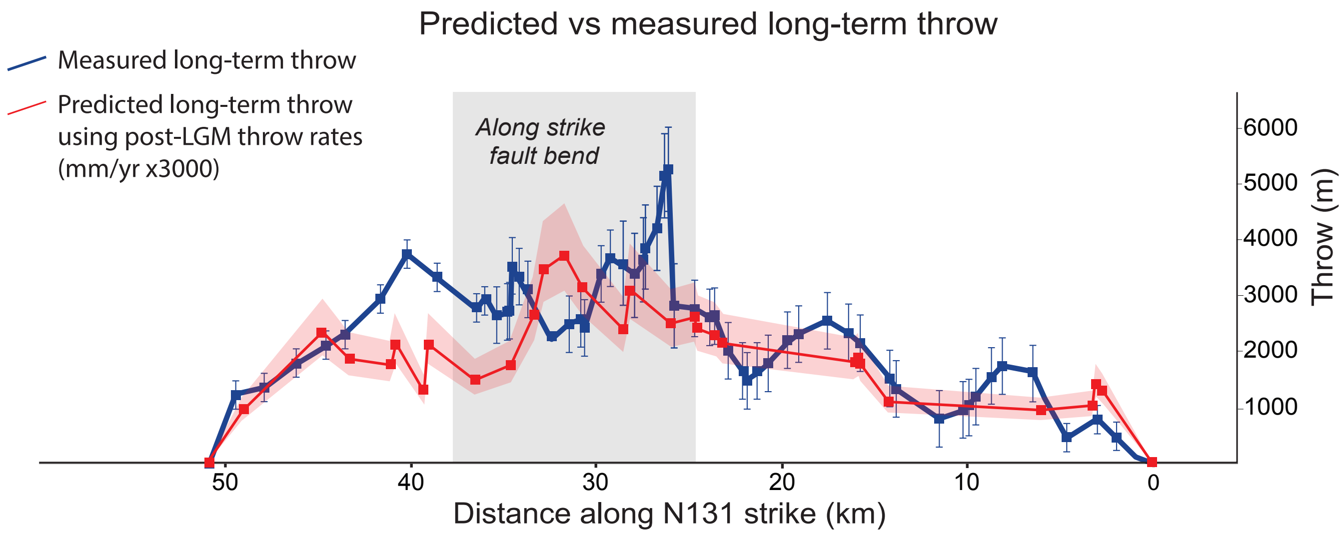
Predicted vs measured long-term throw
Measured long-term throw
Predicted long-term throw
using post-LGM throw rates
(mm/yr x3000)
Along strike
fault bend
6000
5000
4000
3000
2000
1000
Throw (m)
50
40
30
20
10
0
Distance along N131 strike (km)

Figure 11

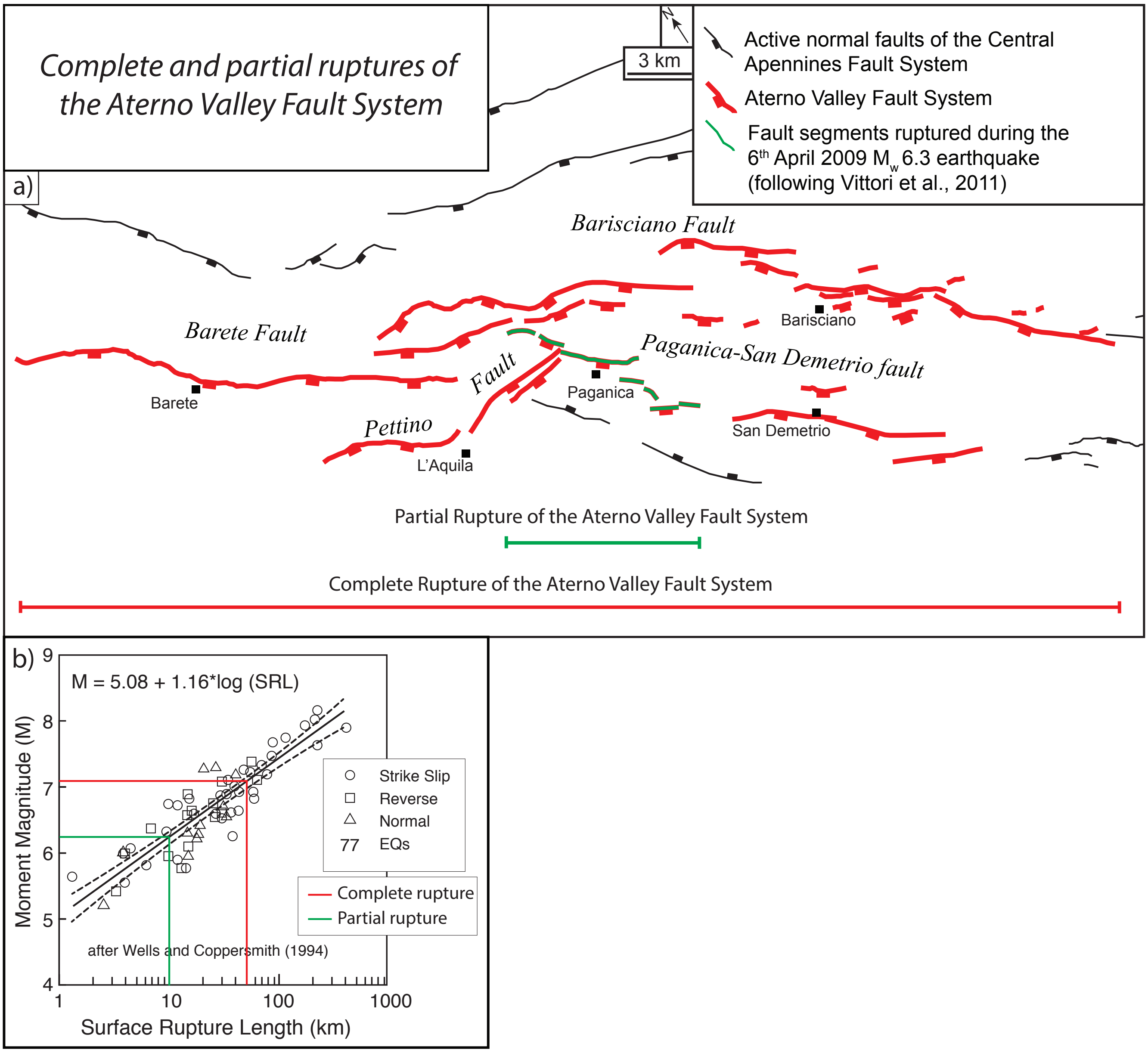

Complete and partial ruptures of the Aterno Valley Fault System
a)
3 km
N
Active normal faults of the Central Apennines Fault System
Aterno Valley Fault System
Fault segments ruptured during the 6th April 2009 Mw 6.3 earthquake (following Vittori et al., 2011)
Barisciano Fault
Barete Fault
Barisciano
Paganica-San Demetrio fault
Fault
Barete
Paganica
Pettino
San Demetrio
L'Aquila
Partial Rupture of the Aterno Valley Fault System
Complete Rupture of the Aterno Valley Fault System
b)
M = 5.08 + 1.16*log (SRL)
Strike Slip
Reverse
Normal
77 EQs
Complete rupture
Partial rupture
after Wells and Coppersmith (1994)
Moment Magnitude (M)
Surface Rupture Length (km)